HHS Public Access

Author manuscript

Cell Rep. Author manuscript; available in PMC 2023 October 23.

Published in final edited form as:

Cell Rep. 2023 April 25; 42(4): 112314. doi:10.1016/j.celrep.2023.112314.

Targeting protein tyrosine phosphatases for CDK6-induced immunotherapy resistance

Xueliang Gao[1,2,12,*], **Yongxia Wu**[3,11,12], **Joel M. Chick**[4], **Andrea Abbott**[2,5], **Baishan Jiang**[6], **David J. Wang**[2], **Susana Comte-Walters**[1], **Roger H. Johnson**[7,8], **Nathaniel Oberholtzer**[5], **Michael I. Nishimura**[9], **Steven P. Gygi**[4], **Anand Mehta**[1,2], **Denis C. Guttridge**[2], **Lauren Ball**[1], **Shikhar Mehrotra**[2,5], **Piotr Sicinski**[6,10], **Xue-Zhong Yu**[2,3,11], **Haizhen Wang**[1,2,13,*]

[1]Department of Cell and Molecular Pharmacology & Experimental Therapeutics, Medical University of South Carolina, Charleston, SC 29425, USA

[2]Hollings Cancer Center, Medical University of South Carolina, Charleston, SC 29425, USA

[3]Department of Microbiology and Immunology, Medical University of South Carolina, Charleston, SC 29425, USA

[4]Department of Cell Biology, Harvard Medical School, Boston, MA 02215, USA

[5]Department of Surgery, Medical University of South Carolina, Charleston, SC 29425, USA

[6]Department of Cancer Biology, Dana-Farber Cancer Institute, and Harvard Medical School, Boston, MA 02215, USA

[8]Cancer Center, Medical College of Wisconsin, Milwaukee, WI 53226, USA

[7]Department of Biophysics, Medical College of Wisconsin, Milwaukee, WI 53226, USA

[9]Department of Surgery, Loyola University Chicago, Maywood, IL 60153, USA

[10]Department of Genetics, Blavatnik Institute, Harvard Medical School, Boston, MA 02215, USA

[11]Present address: Cancer Center, Medical College of Wisconsin, Milwaukee, WI 53226, USA

[12]These authors contributed equally

[13]Lead contact

SUMMARY

[*]Correspondence: gaox@musc.edu (X.G.), wangha@musc.edu (H.W.).

AUTHOR CONTRIBUTIONS

X.G. and H.W. conceived and designed experiments. X.G., Y.W., S.C.-W., J.M.C., and H.W. performed the experiments with help from colleagues. B.J. helped with drug preparation. N.O., M.I.N., and S.M. provided CAR T cells. A.A., D.J.W., R.H.J., S.P.G., A.M., D.C.G., L.B., P.S., and X.-Z.Y. provided advisory support. X.G. and H.W. wrote the manuscript with all authors' input. X.G. and H.W. supervised the project.

DECLARATION OF INTERESTS

P.S. has been a consultant at Novartis, Genovis, Guidepoint, The Planning Shop, ORIC Pharmaceuticals, Cedilla Therapeutics, Syros Pharmaceuticals, and Exo Therapeutics; his laboratory has received funding from Novartis.

SUPPLEMENTAL INFORMATION

Supplemental information can be found online at https://doi.org/10.1016/j.celrep.2023.112314.

Elucidating the mechanisms of resistance to immunotherapy and developing strategies to improve its efficacy are challenging goals. Bioinformatics analysis demonstrates that high CDK6 expression in melanoma is associated with poor progression-free survival of patients receiving single-agent immunotherapy. Depletion of CDK6 or cyclin D3 (but not of CDK4, cyclin D1, or D2) in cells of the tumor microenvironment inhibits tumor growth. CDK6 depletion reshapes the tumor immune microenvironment, and the host anti-tumor effect depends on cyclin D3/CDK6-expressing $CD8^+$ and $CD4^+$ T cells. This occurs by CDK6 phosphorylating and increasing the activities of PTP1B and T cell protein tyrosine phosphatase (TCPTP), which, in turn, decreases tyrosine phosphorylation of CD3ζ, reducing the signal transduction for T cell activation. Administration of a PTP1B and TCPTP inhibitor prove more efficacious than using a CDK6 degrader in enhancing T cell-mediated immunotherapy. Targeting protein tyrosine phosphatases (PTPs) might be an effective strategy for cancer patients who resist immunotherapy treatment.

Graphical Abstract

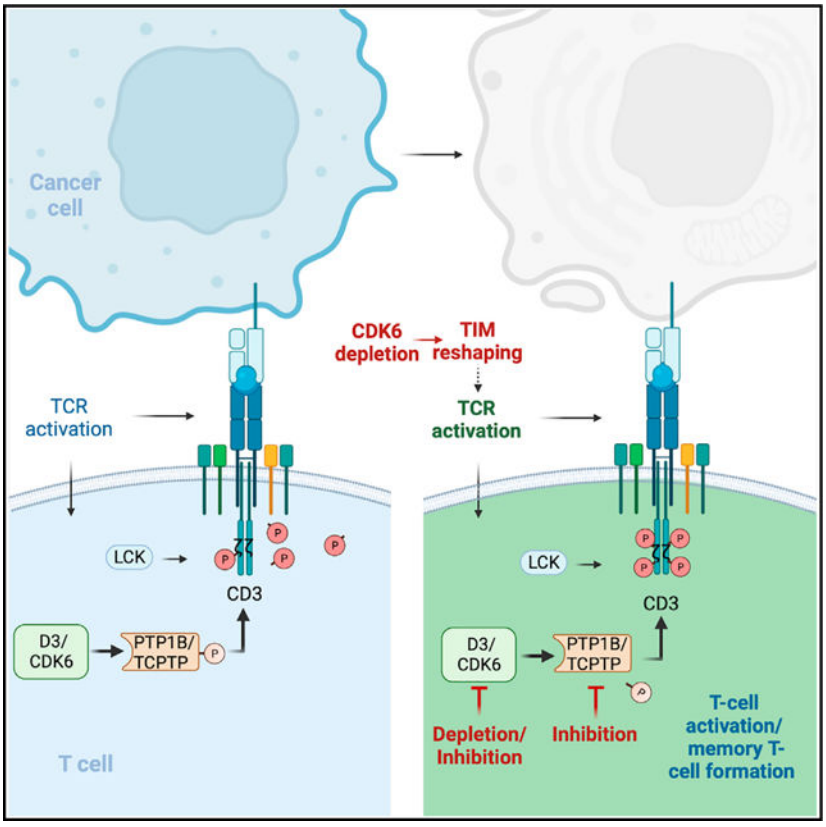

In brief

Using genetic and pharmaceutical approaches, Gao et al. investigate the distinct roles of CDK4 and CDK6 in the TME to regulate tumor growth and evaluate the therapeutic potential of the CDK6-PTP-CD3ζ axis in adoptive T cell therapy.

INTRODUCTION

Although immunotherapy can bring long-lasting clinical benefits, only a fraction of cancer patients respond.[1] To devise effective immunotherapy strategies, it is critical to identify immunotherapy response biomarkers and resistance regulators. CDK4 and CDK6 are cyclin D-dependent kinases functioning in the transition of cell cycle G1-S phase via phosphorylating Rb protein.[2–6] The significant and well-studied roles of CDK4/6 in cancer cells that contribute to tumor progression form the basis for the clinical application of CDK4/6 dual inhibitors in multiple types of cancer.[7–19] The important functions of cyclin Ds in tumorigenesis have also been studied extensively recently.[19–27] However, whether or how cyclin D/CDK4/6 expression in cells of the tumor microenvironment (TME) affects tumor growth and/or the efficacy of immunotherapy remains to be determined.

Although the benefits of CDK4/6 dual inhibitors have been borne out in numerous positive clinical trials, hematological/non-hematological adverse effects and acquired resistance have been documented.[7,20–27] Elucidating the distinct and unknown functions of CDK6 vs. CDK4 could represent a strategy to improve medication compliance. Despite their high functional homology in cell cycle progression, evidence shows that the cellular functions of CDK6 differ from those of CDK4 in regulating cancer cell glycolysis, CXCR4 expression, and PD-L1 stability.[28–30] Cells in the TME play important roles in regulating tumor progression.[31,32] In this study, we investigated the different biological roles of CDK4 and CDK6 in the TME that regulate tumor growth.

T cells play critical roles in regulating tumor progression when they are primed/activated.[33] Cluster of differentiation 3 (CD3), a T cell coreceptor, plays fundamental roles in activating T cells. CD3 is composed of four distinct chains: CD3γ, CD3δ, CD3ε, and CD3ζ. CD3ζ is an essential component in the CD3 protein complex, which has three immunoreceptor tyrosine-based activation motifs (ITAMs) in its cytoplasmic domain. ITAMs are tyrosine phosphorylated following stimulation of the TCR/CD3 complex to convey the activation signals in T cells.[34–36] Whether cytosolic protein tyrosine phosphatases (PTPs) directly regulate the phosphorylation/activities of CD3ζ is not known, although this function has been described to regulate TCR signaling in mice.[37]

In this study, we report that high CDK6 expression positively correlates with immunotherapy resistance in 6 of 7 single-agent immunotherapy clinical studies for melanoma patients. CDK6 depletion, but not that of CDK4, cyclin D1, or D2, in cells of the TME inhibits tumor growth. Mechanistically, this occurs by CDK6 directly phosphorylating and activating PTP1B and T cell PTP (TCPTP) to decrease CD3ζ tyrosine phosphorylation in ITAMs and consequently reduce T cell activities. Our data demonstrate that targeting PTP1B and TCPTP enhances T cell activities and significantly enhances the efficacy of adoptive T cell therapy, which seems superior to targeting CDK6. Cumulatively, these results point to a potentially promising strategy for targeting PTPs as a method to improve the efficacy of immunotherapy for cancer patients.

RESULTS

High CDK6 expression correlates with immunotherapy resistance, and ablation of cyclin D3 or CDK6, but not cyclin D1, D2, or CDK4, in the TME inhibits tumor growth

Gene signatures can serve as reliable biomarkers to predict immunotherapy response.[38] Through clinical data analysis using Tumor Immune Dysfunction and Exclusion (TIDE) software,[38] we found that expression levels of CDK6 and CDK4, but not cyclin D1, cyclin D2, or cyclin D3, were positively correlated with single-agent immunotherapy resistance in 6 of 7 melanoma clinical studies (Figure 1A; Table S1). Among those, CDK6 expression was significantly associated with poor progression-free survival (PFS) in two studies that used either anti-PD1 antibodies (Abs) or adoptive T cell therapy (Figures 1B and S1A). CDK4 expression was not significantly associated with PFS in any study. This suggests that CDK6 may regulate immunotherapy resistance.

Gene signatures are not restricted to genes expressed by tumor cells but can extend to cells in the TME.[38,39] We applied the Gene module in the TIMER1 software to analyze expression levels of cyclin Ds, CDK4, and CDK6 in melanoma samples (SKCM-metastasis).[40] The results showed that CDK4 is more abundantly expressed in tumor cells than in the TME, while the reverse occurs for cyclin D2. Expression levels of CDK6, cyclin D1, and cyclin D3 are nearly equal between the tumor and TME (Figure S1B). Because CDK6 expression in tumors is positively correlated with resistance to immunotherapy (Figures 1B and S1A), we asked whether CDK6 plays a role in the TME to promote tumor growth and decrease the efficacy of immunotherapy. We applied a CDK6 knockout (KO) mouse model to examine wild-type (WT) tumor growth in mice lacking CDK6 in cells of the TME (Figure S1C, left panel). Syngeneic mouse models were established by subcutaneously implanting MC38 cells into CDK6 KO mice. A similar analysis was performed in parallel with CDK4 KO mice. Notably, MC38 tumor growth in CDK6 but not CDK4 KO mice was significantly inhibited compared with WT littermates (Figures 1C and 1D). Tumor-bearing CDK6 KO mice showed prolonged survival with slower tumor growth compared with either WT mice or mice with heterozygous deletion of CDK6 (Figures 1E, 1F, and S1D). The inhibition of tumor growth in CDK6 KO mice was further confirmed using B16F10 cells (Figure S1E). Tumor growth was slowed in CDK6 KO mice, significantly prolonging their survival compared with WT mice (Figures 1G and 1H). Thus, we conclude that the absence of CDK6 in the TME inhibited tumor growth. Because the cell-cycle kinase activity of CDK4/6 depends on their associated cyclin D partners, we also tested tumor growth in cyclin D KO mice (Figure S1C, right panels). Tumor growth was significantly inhibited in cyclin D3 but not in D1 or D2 KO mice (Figures S1F–S1H). These results indicate that expression of CDK6 and cyclin D3 in the TME play important roles in facilitating tumor growth.

CDK6 depletion in the TME reshapes the tumor immune microenvironment and increases tumor-infiltrating T cell cytotoxicity

Comparing the subpopulations of cells in the TME in MC38 tumors from CDK6 KO vs. WT mice (Figure S8A, gating strategies), we observed that the natural killer (NK) cell population was significantly increased in CDK6 KO mice (Figures 2A and S2A).

No significant differences in the frequencies of B cells, macrophages, dendritic cells, MDSCs, or T cells ($CD8^+$, $CD4^+$, or Treg) were found (Figures 2B–2G and S2B–S2G). Remarkably, the frequencies of central memory T (Tcm) cells ($CD62L^{High}CD44^{High}$) and effector memory T (Tem) cells ($CD62L^{Low}CD44^{High}$) were significantly increased in tumors from CDK6 KO mice (Figures 2H, 2I, and S8B, gating strategies). Increased cytokine production of interferon-γ (IFN-γ) and granzyme B (GzmB) reflects enhanced cytotoxic T cell activation.[41,42] Expression levels of IFN-γ, GzmB, and tumor necrosis factor alpha (TNF-α) in $CD8^+$ T cells among the tumor-infiltrating lymphocytes (TILs) were significantly increased in CDK6 KO compared with WT mice (Figures 2J–2L). The expression levels of IFN-γ and GzmB were also significantly increased in CDK6 KO tumor-infiltrating $CD4^+$ T cells (Figures 2M–2O). In addition, cell proliferation ($Ki67^+$) of TILs was not significantly affected upon CDK6 depletion (Figure S2H). The expression levels of IFN-γ and GzmB in TILs from CDK4 KO mice were not significantly changed compared with the WT (Figures S2I–S2N). These data suggest that depletion of CDK6 in the TME reshapes the tumor immune microenvironment and activates T cells to inhibit tumor growth.

Depletion of $CD8^+$ or $CD4^+$ T cells, but not NK cells, reverses the host antitumor effects of CDK6 KO mice

Given their important role in anti-tumor immunity,[43,44] we next addressed the anti-tumor contribution of $CD8^+$ T cells in CDK6 KO mice. Anti-CD8 monoclonal Abs (mAbs) were injected intraperitoneally to deplete $CD8^+$ T cells (Figure 3A), as confirmed by fluorescence-activated cell sorting (FACS) prior to tumor inoculation (Figure 3B). Pre-depleting $CD8^+$ T cells completely reversed the host anti-tumor effects of CDK6 KO (Figure 3C).

These data clearly demonstrate that the antitumor activity seen in CDK6 KO mice is $CD8^+$ T cell-dependent. We similarly depleted $CD4^+$ T cells with anti-CD4 mAbs and examined tumor growth in CDK6 KO mice (Figure 3D). Pre-depleting $CD4^+$ T cells also reversed the host anti-tumor effects of CDK6 KO (Figures 3E and 3F). In addition, we confirmed that CDK4 and CDK6, together with cyclin D2 and cyclin D3, were highly expressed in activated T cells in which cyclin D1 was barely expressed (Figure S2O). The deletion of CDK6 or CDK4 in splenic T cells isolated from CDK6 or CDK4 KO mice was further confirmed by immunoblotting (Figure S2P). Although CDK4/6 inhibition (palbociclib treatment) arrests splenic T cells at the G0/G1 phase, CDK6 depletion in T cells did not significantly affect cell cycle progression (Figure S2Q). This suggests that the presence of CDK4 alone in CDK6-depleted T cells might be sufficient to promote cell cycle progression and sustain cell proliferation.

NK cells can kill tumor cells and prime T cells via processing/presenting antigens, secreting cytokines, and regulating dendritic cell antigen presentation.[45–48] The population of tumor-infiltrating NK cells was significantly increased in CDK6 KO mice (Figure 2A). NK cells are reported to constrain tumor growth at a very early stage.[49] Thus, we also examined the roles of NK cells in suppressing tumor growth in these animals. Anti-NK1.1 Abs were injected intraperitoneally to pre-deplete NK cells (Figure 3G). The FACS results confirmed

NK cell depletion before tumor implantation and at the end of experiments (Figures 3H and S3A). However, pre-depleting NK cells did not reverse the host anti-tumor effects of CDK6 KO (Figure 3I), demonstrating that NK cell depletion alone is not sufficient to reverse the host antitumor activity in CDK6 KO mice.

Adoptive transfer of antigen-activated CDK6-depleted T cells enhances survival of tumor-bearing mice

We next asked whether CDK6 depletion in T cells increases T cell activities to suppress tumor growth. Intrinsic CDK6 deletion in T cells using the CD4-CRE system does not inhibit tumor growth.[50] Lack of costimulatory signaling may lead to immunological ignorance, as evidenced by several T cell receptor (TCR) transgenic models, while the anti-tumor effects are significantly enhanced when transgenic T cells are activated *in vitro* before cells are adoptively transferred into the host.[51–54] Thus, to determine whether CDK6 depletion in TCR-activated T cells enhances tumor suppression efficacy after adoptive transfer, we generated CDK6 KO OT-I mice by crossing OT-I transgenic mice with CDK6 KO mice. The $CD8^+$ T cells from OT-I mice expressing transgenic TCR are designed to recognize ovalbumin (OVA) residues 257–264. Indeed, intravenous (i.v.) injection of CDK6 KO OT-I $CD8^+$ T cells showed significantly enhanced anti-tumor efficacy compared with WT OT-I $CD8^+$ T cells (Figures 3J, 3K, S3B, and S3C). The enhanced anti-tumor efficacy of CDK6 KO $CD8^+$ T cells was further confirmed by performing an additional *in vivo* experiment on B16F10-OVA tumors (Figures 3L and S3D). These data suggest that CDK6 depletion in antigen-activated T cells enhances the efficacy of tumor suppression.

CDK6 inhibition increases tyrosine phosphorylation of proteins functioning in TCR signaling

To systematically interrogate the mechanism underlying CDK6 regulation of T cell activity, we performed a tandem mass tag mass spectrometry (TMT-MS)-based comparative analysis of KOPTK1 leukemia T cells with and without treatment of the CDK4/6 dual inhibitor palbociclib. The effects of palbociclib treatment on this T-ALL cell line mainly reflect an inhibitory effect on CDK6 that is highly expressed in leukemia T cells, in contrast to CDK4, which is barely expressed.[30] CDK6 kinase phosphorylates substrates at serine/threonine proline (S/TP) sites.[55] Interestingly, TMT-MS analysis showed not only decreased serine/threonine phosphorylation of proteins but also an increase in phosphorylation of tyrosine residues in 105 proteins. Gene Ontology (GO) enrichment analysis in BP terms (DAVID 6.8) showed that “T cell receptor signaling pathway” was the top-ranked annotation group among increased tyrosine-phosphorylated proteins (Figure 4A; Tables S2 and S3). These results suggest that CDK6 inhibition may enhance T cell activity by increasing tyrosine phosphorylation of proteins functioning in the T cell receptor signaling pathway. Tyrosine phosphorylation of proteins is regulated by tyrosine kinases and PTPs.[56] We found that several PTPs displayed decreased phosphorylation at CDK-dependent S/TP sites upon treatment with palbociclib (Figures 4B; Table S4). These data and analyses suggest that CDK6 inhibition may dephosphorylate/inactivate tyrosine phosphatases to increase tyrosine phosphorylation of their substrates to activate T cells.

Cyclin D3/CDK6 phosphorylates/activates PTP1B and TCPTP

The identified PTPs that displayed decreased phosphorylation at S/TP sites upon CDK6 inhibition include TCPTP and PTP1B, two important non-receptor intracellular PTPs highly expressed in hematopoietic tissues.[57–59] Immunoblotting verified decreased phosphorylation of PTP1B and TCPTP in CDK6-inhibited leukemia T cells (Figure 4C), CDK6 degrader-treated WT mouse splenic $CD8^+$ T cells, and CDK6 KO $CD8^+$ T cells but not in CDK4 KO $CD8^+$ T cells (Figure 4D). To examine how CDK6 inhibition affects PTP1B and TCPTP phosphatase activities, we individually immunoprecipitated these proteins from lysates of Jurkat T cells treated with a CDK4/6 inhibitor or CDK6 degrader. Of note, CDK4/6 inhibitor or CDK6 degrader treatment significantly decreased the phosphatase activities of PTP1B and TCPTP (Figure 4E). The selective CDK6 degrader BSJ-03–123 was applied,[60] and its efficiency and specificity were validated (Figure S4A). In addition, the S/TP phosphorylation and phosphatase activities of PTPs were decreased in CDK6 but not CDK4 knockdown T cells (Figures S4B and S4C), suggesting that the regulation of PTPs is specific to CDK6.

In vitro kinase assays showed that PTP1B and TCPTP were specifically phosphorylated by cyclin D3/CDK6 (Figure 4F). Cyclin D2 and CDK4, together with cyclin D3 and CDK6, are also expressed in activated T cells[61] (Figure S2O). The results of *in vitro* kinase assays showed that only cyclin D3/CDK6, but not other cyclin D/CDK combinations, can directly phosphorylate PTP1B and TCPTP (Figures S4D and S4E, respectively). Of note, the phosphatase activities of PTP1B and TCPTP were significantly enhanced when they were phosphorylated by CDK6 *in vitro* (Figure 4G).

Our TMT-MS analysis showed that Ser50 in PTP1B and Ser304 in TCPTP were dephosphorylated in T cells treated with palbociclib (Figure 4B). To identify the serine/threonine sites in PTP1B and TCPTP phosphorylated by cyclin D3/CDK6, we further performed MS-based phosphorylation analysis of recombinant PTP1B and TCPTP proteins after *in vitro* protein kinase assays. The results showed that multiple residues were phosphorylated by cyclin D3/CDK6 (Figures S4F and S4G; Table S5). Immunoblotting following the kinase assay showed that S50 and S205 are two major residues on PTP1B phosphorylated by cyclin D3/CDK6 because the 2SA-PTP1B mutant (S50, S205 to alanine) was no longer phosphorylated by cyclin D3/CDK6. We also conclude that S52, T261, S298, and S304 are four major residues on TCPTP phosphorylated by cyclin D3/CDK6 because the 4SA-TCPTP mutant (S52, T261, S298, and S304 to alanine) was no longer phosphorylated by cyclin D3/CDK6 (Figures 4H and S4H). Furthermore, *in vitro* phosphatase assays showed that alanine mutants of PTPs (S50A-, 2SA-PTP1B and S52A-, 4SA-TCPTP) had significantly lower phosphatase activities compared with WT PTPs post kinase assays with cyclin D3/CDK6 (Figure 4I). Without phosphorylation by cyclin D3/CDK6, alanine mutants of PTPs showed similar phosphatase activities as the WT (Figure S4I). These findings suggest that cyclin D3/CDK6 phosphorylates PTP1B and TCPTP to increase their phosphatase activities in T cells. Besides PTP1B and TCPTP, our TMT-MS data showed that the phosphorylation of PTPRA and PPM1D also decreased in T cells treated with palbociclib. Although the S/TP phosphorylation of PTPRA and PPM1D was decreased in CDK6-depleted T cells, their phosphatase activities were not significantly

changed (Figure S4J). This result suggests CDK6 specifically regulates the phosphatase activities of PTP1B and TCPTP but not other PTPs.

CDK6 inhibition increases CD3ζ tyrosine phosphorylation mediated by PTP1B and TCPTP

The above results indicate that CDK6 inhibition may enhance T cell activity by inactivating PTP1B and TCPTP (PTPs) to increase tyrosine phosphorylation of proteins functioning in the T cell receptor signaling pathway, including CD3. Our TMT-MS data showed that CDK6 inhibition causes an increase in tyrosine phosphorylation at ITAMs of CD3ε and CD3γ (Table S2). We confirmed the enhanced tyrosine phosphorylation of CD3ε and CD3γ by immunoblotting using the phospho-tyrosine Ab pY99 (Figures 5A and 5B). CD3ζ tyrosine phosphorylation at ITAMs is an indicator of T cell activation. Immunoblotting using pY99 Abs and flow cytometry using phospho-CD3ζ (Tyr142) Abs confirmed that tyrosine phosphorylation of CD3ζ was also increased when CDK6 was inhibited by palbociclib in Jurkat cells (Figures 5C and 5D).

To examine whether PTP1B and/or TCPTP directly dephosphorylate CD3 subunits, we immunoprecipitated CD3ε, CD3γ, and CD3ζ individually from lysates of Jurkat cells to perform a phosphatase assay with active recombinant PTP1B or TCPTP proteins. This *in vitro* phosphatase assay showed that CD3ε was dephosphorylated by PTP1B (Figure 5E), and CD3γ was dephosphorylated by TCPTP (Figure 5F). Importantly, CD3ζ was dephosphorylated by PTP1B and TCPTP (Figure 5G). Going forward, in this study, we focused on CD3ζ because of its significance in T cell activation. To investigate the effect of CDK6 inhibition on regulating the phosphatase activities of PTPs to modulate CD3ζ tyrosine phosphorylation, we immunoprecipitated PTP1B or TCPTP individually from lysates of Jurkat cells with or without palbociclib treatment to perform *in vitro* phosphatase assays. We first confirmed that palbociclib treatment decreased S/TP phosphorylation of PTP1B and TCPTP (Figure 5H, lower). LCK, a critical kinase, phosphorylates CD3ζ to activate T cells.[62–64] CD3ζ phosphorylated by LCK was applied as the specific substrate for PTP1B and TCPTP (Figure S5A). Immunoblotting results following the phosphatase assays showed that tyrosine phosphorylation of CD3ζ is less dephosphorylated by PTP1B or TCPTP immunoprecipitated from T cells treated with palbociclib compared with the dephosphorylation by PTPs from untreated T cells (Figure 5H, top). This suggested that CDK6 inhibition dephosphorylates PTP1B and TCPTP in T cells and therefore inactivates their phosphatase activity on CD3ζ. To test whether PTP1B and TCPTP dephosphorylate CD3ζ *in vivo*, we treated Jurkat cells with PTP1B-IN2 (1 μM to inhibit PTP1B and TCPTP[65]) and then measured the tyrosine phosphorylation of CD3ζ. Immunoblot results showed that tyrosine phosphorylation of CD3ζ was significantly increased when PTP1B and TCPTP were inhibited (Figures 5I and S5B). Compared with WT T cells, increased tyrosine phosphorylation of CD3ζ was consistently observed in mouse T cells in which CDK6 was knocked out or inhibited (Figures 5J–5L and S5C). In accordance with the data from murine T cells, these results were also observed in human T cells in which PTPs were inhibited or cyclin D3/CDK6 was inhibited or depleted (Figures 5M, 5N, and S5D). SHP-1 and SHP-2 are the known phosphatases for CD3ζ.[66] We excluded the possibility that CDK6 phosphorylates SHP-1 and/or SHP-2 to decrease CD3ζ tyrosine phosphorylation because neither the CDK-dependent S/TP phosphorylation levels of SHP-1/SHP-2 nor their

phosphatase activities were significantly changed under CDK6 inhibition (Figures S5E and S5F). Thus, we conclude that CD3ζ is a target of PTP1B and TCPTP and that inhibiting or depleting CDK6 increases CD3ζ phosphorylation as a result of PTP1B and TCPTP inactivation.

CDK6 depletion or PTP1B/TCPTP inhibition increases cytokine production in T cells

Next, we measured cytokine expression to test whether directly targeting the CDK6-PTPs-CD3ζ axis in T cells enhances T cell activities. CDK6 degrader treatment significantly reduced CDK6 expression in $CD8^+$ T cells (Figure S5C). Correspondingly, CD3ζ phosphorylation (Figures 5K and 5L) and IFN-γ and GzmB production were significantly increased (Figures 6A and 6B). In primary human T cells, results consistently revealed that PTP1B/TCPTP or cyclin D3/CDK6 inhibition/depletion led to CD3ζ tyrosine phosphorylation (Figures 5M and 5N) and increased production of IFN-γ and GzmB (Figures 6C–6F). It is noteworthy that CDK6 inhibition/depletion or PTP inhibition increased T cell differentiation to memory T cells (Figure 6G) without dramatically affecting T cell proliferation (Figure S6A).

Further, we demonstrated that CD3ζ tyrosine phosphorylation mediated the cytokine upregulation in CDK6 inhibited/depleted T cells. The LCK kinase inhibitor PP2 was applied to treat mouse T cells to prevent CD3ζ phosphorylation. Flow cytometry results showed that PP2 treatment decreased CD3ζ tyrosine phosphorylation to similar levels in WT and CDK6 KO T cells (Figure 6H). As a consequence, the increase in production of IFN-γ, GzmB, and TNF-α was attenuated in CDK6 KO T cells upon treatment with PP2 (Figures 6I, 6J, and S6B). This suggests that the increased cytokine production induced by CDK6 depletion depends on CD3ζ phosphorylation. We proceeded to test whether the activities of PTP1B and TCPTP mediated the enhanced CDK6-regulated cytokine production in T cells. Treating mouse CDK6 KO T cells with a PTP inhibitor increased CD3ζ tyrosine phosphorylation and cytokine expression to a similar level as seen in WT cells (Figures 6H–6J). To test whether PTP1B and TCPTP are required for CDK6-regulated cytokine production and CD3ζ phosphorylation, we knocked down PTP1B and TCPTP in T cells (Figure S6C). IFN-γ/GzmB production and CD3ζ phosphorylation were increased in these PTP knockdown cells. CDK6 inhibition/depletion by palbociclib or CDK6 degrader treatment did not further increase the enhanced IFN-γ/GzmB production and CD3ζ phosphorylation in PTPs knockdown cells (Figures 6K–6M). In addition, PTP1B and TCPTP alanine mutant-expressing cells showed higher cytokine production and CD3ζ phosphorylation compared with WT PTPs. CDK6 inhibition/depletion in cells expressing the alanine-mutant PTPs did not further increase their cytokine production and CD3ζ phosphorylation (Figures 6N–6P and S6D). In all, these experiments demonstrated that the upregulated cytokine production subsequent to CDK6 inhibition/depletion depends on CD3ζ tyrosine phosphorylation, which is mediated by the phosphatase activity and CDK6-specific phosphorylation of PTP1B and TCPTP. In total, these observations support the conclusions that (1) cyclin D3/CDK6 phosphorylates/activates PTP1B and TCPTP to dephosphorylate CD3ζ and suppress T cell activation and memory T cell differentiation and that (2) targeting the CDK6-PTPs axis enhances T cell activities.

Targeting PTPs enhances the efficacy of T cell killing and adoptive T cell immunotherapy

Next, we examined the anti-tumor efficacy of targeting the CDK6-PTPs axis in $CD8^+$ T cells. B16F10 cells expressing OVA (B16F10-OVA) were co-cultured with $OVA_{257–264}$ peptide pre-stimulated $CD8^+$ T cells isolated from OT-I mice. PTP1B/TCPTP inhibition or CDK6 inhibition/depletion treatment significantly enhanced the tumor-killing capability of $CD8^+$ T cells (Figure 7A). CDK6 depletion did not enable PTP1B/TCPTP inhibitor-treated $CD8^+$ T cells to further increase their enhanced tumor-killing capacity (Figures S7A and S7B), suggesting that the CDK6 depletion-induced T cell killing capacity is mediated through PTPs. The enhanced tumor-killing capability of $CD8^+$ T cells upon PTP1B/TCPTP inhibition was also observed on MC38-OVA cells (Figure S7C). An *in vitro* CAR T cell killing assay was applied to test CDK6- or PTP1B/TCPTP-regulated human T cell activities. To assess tumor killing capacity, Raji cells expressing CD19 and GFP were co-cultured with CD19 CAR T cells. The co-cultured cells were then treated with a CDK6 degrader, PTP inhibitor, or vehicle. Cytotoxicity was determined as the percentage of apoptotic Raji cells. Consistent with the results from mouse T cells, CDK6 degrader or PTP inhibitor treatment significantly increased the apoptotic Raji cell populations in the CAR T cell co-culture group (Figure 7B). No significant change of apoptotic cells was observed when Raji cells were treated with a CDK6 degrader or PTPs inhibitor in the absence of CAR T cells (Figure S7D). These results indicate that CDK6 depletion or PTP inhibition increases CAR T cells' tumor-cell-killing capacity. CDK6 depletion in PTP inhibitor-treated CAR T cells did not further increase their enhanced tumor-killing capacity (Figure 7B). This again suggests that the CDK6 depletion-induced CAR T cell tumor-killing capacity is mediated through PTPs.

We then tested whether administration of a PTP inhibitor or CDK6 degrader can augment the anti-tumor activity of $CD8^+$ T cells *in vivo*. Splenic $CD8^+$ T cells from OT-I mice were adoptively transferred by i.v. injection to sub-lethally irradiated B16F10-OVA tumor-bearing C57BL/6-Ly5.1 mice (Figure S7E). Administration of a PTP inhibitor or CDK6 degrader significantly enhanced the host anti-tumor efficacy, as evidenced by reduced tumor growth, which was also observed in the control palbociclib group (Figures 7C and S7F). The expression levels of IFN-γ and GzmB in $CD8^+$ T cells and the populations of Tcm cells were significantly increased in TILs from mice receiving PTP inhibitor treatment (Figure 7D).

To test whether blocking the CDK6-PTPs axis augments the anti-tumor activity of CAR T cells *in vivo*, we administrated a CDK6 degrader or PTP inhibitor to Raji tumor-bearing NSG mice receiving human CAR T cell treatment. The PTP inhibitor can significantly augment the killing efficacy of CAR T cells, as indicated by bioluminescence imaging-monitored tumor progression and overall survival of tumor-bearing mice (Figures 7E and 7F). The PTP inhibitor showed a better therapeutic effect than the CDK6 degrader during the first 3.5 weeks (~day 24) (Figure S7G). The Raji tumor ultimately progressed/relapsed, possibly because of loss of CD19 or a decrease in the CAR T cell population. In addition, without CAR T cells, PTPs inhibitor treatment did not significantly affect tumor progression and the overall survival of tumor-bearing mice (Figures 7F and S7H). We also tested whether targeting PTPs *in vivo* enhances anti-tumor responses following immunotherapy with checkpoint blockade. The PTP inhibitor treatment improved the overall survival of

B16F10 tumor-bearing mice receiving PD-L1 Ab treatment, which suggests that the PTP inhibitor may augment the efficacy of checkpoint blockade in immunologically cold tumors (Figure S7I).

Targeting PTPs shows superior persistence in preventing tumor growth compared with targeting CDK6

We further applied a melanoma adoptive cell transfer (ACT) model to assess the anti-tumor effect of the PTP inhibitor PTP1B-IN2. In this model, splenic $CD8^+$ T cells from pmel mice were adoptively transferred to sub-lethally irradiated B16F10 tumor-bearing C57BL/6 mice (Figure S7J). Because our study showed that PTP inhibitor treatment enhanced the memory T cell population in the B16F10-OVA (Figure 7D, bottom panels) and Raji-CAR-T mouse models (Figure 7G), we went on to test the persistence of the observed PTP inhibitor-induced anti-tumor effect. To this end, we treated tumor-recipient mice with PTP1B-IN2 or a CDK6 degrader for 3 weeks, discontinuing treatment when the tumors in control mice receiving pmel T cells started to grow. PTP inhibitor treatment significantly augmented the therapeutic efficacy of pmel T cells compared with the CDK6 degrader, as evidenced by superior melanoma growth suppression. The survival probability analysis showed that 4 of 9 mice were alive 11 weeks post treatment in the group receiving PTP inhibitor treatment and ACT compared with 1 of 9 in the group receiving CDK6 degrader and ACT treatment and 0 of 5 in the group receiving ACT treatment alone (Figures 7H, left, and S7K). Tumor-free survival analysis showed that 4 of 9 mice were tumor-free 11 weeks post treatment in the group receiving PTP inhibitor treatment and ACT compared with 1 of 9 in the group receiving CDK6 degrader and ACT treatment and 0 of 5 in the group receiving ACT treatment alone (Figure 7H, right). These results suggest that the PTP inhibitor is significantly more potent than the CDK6 degrader in enhancing the efficacy of ACT immunotherapy in the mouse melanoma model. We did not observe any toxic effects following PTP inhibitor or CDK6 degrader treatment because treated mice had no significant weight loss (Figure S7L) and toxicity profile change (Table S6).

Collectively, these data demonstrate that CDK6 depletion in the TME reshapes the tumor immune microenvironment and increases T cell activities to inhibit tumor growth. Inhibiting CDK6 kinase activity in T cells inactivates PTP1B and TCPTP, activating TCR signaling by upregulating CD3ζ tyrosine phosphorylation and thereby inhibiting tumor growth (Figure 7I). Regarding improving the effectiveness of immunotherapies, our results further suggest that inhibiting PTPs may have better therapeutic efficacy than depleting CDK6 in T cells. Thus, targeting PTPs is a promising strategy to enhance immunotherapy efficacy.

DISCUSSION

Previous studies using CDK4/6 inhibitors showed that targeting CDK4/6 suppresses $CD4^+$ $FOXP3^+$ regulatory T cell proliferation and numbers to promote effector T cell activity,[67] increases T cell activity by suppressing the NFAT protein family and enhances T cell tumor infiltration,[68] and promotes CD8 T cell memory formation.[69,70] Our study showed that depleting CDK6 in the TME significantly increased effector T cell activities and the frequency of tumor-infiltrating NK cells but not the frequencies of other immune cells

(Figures 2A–2G). This suggests that specific depletion of CDK6 in the TME triggers different mechanisms from dual CDK4/6 inhibition to regulate immune cell subpopulations and their activities to augment the anti-tumor response. While it has been reported that CDK6 depletion in T cells alone using the CD4-CRE system is not sufficient to suppress tumor growth,[50] our study showed that CDK6 depletion in all types of cells in the TME inhibited tumor growth via enhancing T cell activity and memory T cell differentiation. CDK6-depleted T cells may need priming from other types of CDK6-depleted immune cells to efficiently suppress tumor growth. Potentially, the increased NK cells, together with other types of immune cells, prime and activate T cells (first step), and then CDK6 depletion in T cells further increases the activities of stimulated T cells to inhibit tumor growth (second step).

We found that cyclin D3/CDK6 phosphorylates and increases the activities of PTP1B and TCPTP to decrease CD3ζ tyrosine phosphorylation and T cell activities. The identified phosphorylation residues Ser50/52, Ser205, and Thr261 are located in close proximity to the catalytic sites/allosteric binding site of PTP1B and TCPTP.[71–73] It is likely that PTP1B/TCPTP phosphorylation by cyclin D3/CDK6 increases their substrate binding capability and/or catalytic activity. It is known that TCR activation leads to memory T cell differentiation,[74,75] which may explain our finding that targeting the CDK6-PTP1B/TCPTP-CD3ζ axis not only increases T cell activity but also promotes memory T cell differentiation. One study, in which phorbol myristate acetate (PMA)/ionomycin was used to activate naive T cells,[50] showed that CDK6 depletion does not regulate protein kinase C (PKC)-stimulated T cell activation. PMA/ionomycin stimulation bypasses early T cell activation steps (i.e., the TCR-CD3 complex and CD3ζ phosphorylation) to directly stimulate a downstream regulator, PKC, to activate T cells.[76,77] This suggests that CDK6 is specifically involved in the early steps of TCR signal transduction but not in the latter steps of T cell activation. Our study showed that targeting PTPs is effective and promising for augmenting ACT and that it might be more efficacious than targeting CDK6 (Figures 7E–7H). The higher therapeutic efficacy of the PTP inhibitor may be due to it hitting PTPs in a variety of immune cell types.[37,78,79]

Recent studies showed that targeting PTP1B and/or TCPTP augments immunotherapy.[80–85] Our study shows that targeting PTP1B and TCPTP using PTP1B-IN2 significantly enhances immunotherapy efficacy with no observable toxicity (Figure S7L; Table S6). Future studies may focus on comparing the therapeutic efficacy of different PTP inhibitors in augmenting immunotherapy.

Limitations of the study

This study used PTPs inhibitors (PTP1B-IN2) to demonstrate their effects on anti-tumor immunity. Future studies may investigate whether the inhibition of PTP1B, of TCPTP, or of both is required for this effect. In *in vivo* CAR T cell experiments, PTP1B-IN2 is more efficacious than BSJ-03–123 at early treatment. The augmented efficacy was gradually lost, possibly because of loss of CAR or CAR T cells because only one dose of CAR T cells was applied. Future studies may increase the doses of CAR T cells to compare the anti-tumor

efficacy of these compounds. In addition, the efficacy of PTP1B-IN2 may be compared with other PTP inhibitors in augmenting immunotherapy in future studies.

STAR★METHODS

RESOURCE AVAILABILITY

Lead contact—Resource and reagent requests should be directed to the lead contact, Haizhen Wang (wangha@musc.edu).

Materials availability—The study did not generate new unique reagents.

Data and code availability

- Adjective data reported in this paper will be shared by the lead contact upon request.
- This paper does not report original code.
- Any additional information required to reanalyze the data reported in this paper is available from the lead contact upon request.

EXPERIMENTAL MODEL AND SUBJECT DETAILS

Mice—CDK6 knockout mice were kindly gifted by Mariano Barbacid at the Spanish National Cancer Research Center. CDK4 knockout mice were gifted by Hiroaki Kiyokawa at Northwestern University. Cyclin D1, cyclin D2, and cyclin D3 individually knockout mice were gifted by Peter Sicinski's group. pmel, C57BL/6 and C57BL/6-Ly5.1 mice (6–8 weeks) were purchased from the Jackson Laboratory. Tumor-bearing mice were randomly grouped to receive control or drug treatments. OT-I transgenic mice (003831) and NSG mice (005557) were purchased from the Jackson Laboratory. Animal procedures adhered to the study protocol approved by the Institutional Animal Care and Use Committee of the Medical University of South Carolina.

For peptide immunization and B16F10 melanoma synergic tumor model establishment, peptide immunization was performed according to published protocols with appropriate modifications.[91–93] Adult CDK6 KO or wild-type mice (male or female >6 weeks) were immunized with 80 nmol of the altered gp100 9-mer peptide (EG*P*RNQDWL) and 80 nmol of the TRP-2 native peptide (TRP-2 180–188 peptide SVYDFFVWL) *via* a subcutaneous injection after shaving part of the left flank. The altered gp100 9-mer peptide was dissolved in PBS. The TRP-2 native peptide was dissolved in DMSO (2%), then in PBS (98%) dropwise, followed by sonication. Immediately following peptide injection, 3 mg imiquimod was topically applied to the skin at the injection site. The immunization procedure was repeated 7 days later. Mice received two I.P. injections of mouse IL-2 (Miltenyi Biotec, 130–120-333, 5×10^4 IU) on the day of the second vaccination, as well as on the following day. 5×10^4 B16F10 melanoma cells were subcutaneously injected into the flank of adult CDK6 KO or wild-type C57BL/6 mice. Tumor sizes were measured twice a week by caliper after implantation, and tumor volume was calculated as (width^{2}X length)/2. For survival studies, animals were monitored for tumor volume twice a week after initial treatment until

tumor volume exceeded 2,000 mm^3. The investigator was not blinded to the allocation of mice to mouse groups.

For adoptive T cell therapy and combined treatment with PTPs inhibitor or CDK6 degrader, Splenic OT-I cells (WT or CDK6 KO) were cultured in the presence of OVA peptides for three days. OT-I cells were washed with PBS and adoptively transferred by I.V. injection to sub-lethally irradiated tumor-bearing mice. For adoptive pmel T cell therapy, splenic pmel T cells were cultured in the presence of $gp100_{(25–33)}$ peptides for three days. Tumor-recipient mice were treated with CDK6 degrader, PTPs inhibitor or palbociclib starting 4 days post T cell transferring as described in timeline figures. For the B16F10-OVA mouse model, mice were treated with the compounds until the end of the experiment, and tumors were collected to analyze T cell activities and memory T cell formation. The pmel mouse model was applied for tumor-free survival analysis, and tumor-recipient mice were treated for three weeks (five times per week). Tumor size was measured 2–3 times per week. For drug treatment, the dose of BSJ-03–123 was 50 mg/kg (I.P. injection), palbociclib was 50 mg/kg (oral gavage), and PTP1B-IN2 was 5 mg/kg (oral gavage) of body weight.

For CD8, CD4 T, or NK cell depletion, anti-CD8, -CD4 or -NK1.1 Abs (200μg/mouse) were I.P. delivered to CDK6 KO mice three days before MC38 cell implantation and every three days thereafter. IgG was applied as a control.

For bioluminescence imaging, NSG mice (6 weeks old female) received 0.5×10^6 Raji-Luc cells in 0.5mL PBS via tail vein injection on Day 0, followed by a tail vein injection of 2×10^6 CAR T cells in 0.5mL PBS on Day 3. The mice were subsequently treated with drugs at D5–23. Mice were subjected to *in vivo* bioluminescence imaging on D8, D17, and D23 using the IVIS 200 imaging system after receiving an intraperitoneal injection of D-luciferin (100 mg/kg body weight). For comparison, the same settings of the IVIS system were applied to all groups on individual days. Exposure time: 40 s on Day 11; 1 s on Day 17; 0.5 s on Day 23. Bioluminescence signals were analyzed with Living Image Software version 4.7.

Cell lines and primary T cells—MC38 and B16F10 were cultured in DMEM, and Jurkat T cells were cultured in RPMI-1640 medium supplemented with 10% FBS and 1% Pen-Strep (100U/mL penicillin,100 μg/mL streptomycin), and cultured at 37°C, 5% CO_2. Human primary T cells were isolated from LRS cones (200–0093) purchased from Stemcell Technologies. None of these cell lines is listed in the Database of Cross-Contaminated or Misidentified Cell Lines.

Cell transfection and virus infection were performed as previously described before with appropriate modifications.[30] In brief, HEK293T cells seeded in 10-cm petri dishes one day before transfection were applied for retroviral and lentiviral plasmids packaging. Polyethylenimine (PEI) was applied for HEK293T transfection. The culture medium with secreted viruses was collected two days after transfection. After filtering through a 0.45 μm filter, high-speed ultracentrifugation was applied to concentrate the virus at 21,000 rpm for 1.5 h. The virus pellet was resuspended in fresh media. Cells were infected with the virus for

24 h in the presence of 5 μg/mL polybrene. After culturing for two days, the corresponding selection reagent was added with fresh cell culture media.

METHOD DETAILS

Immunoprecipitation assay and immunoblot—For immunoprecipitation (IP) assays, 1–2 mg cell lysate in IP lysis buffer (Pierce, 87788) supplemented with protein protease inhibitors (Roche, 11836170001) and phosphatase inhibitors (Roche, 04906837001) were incubated with primary or control antibodies on a rocker platform overnight at 4°C. 30 μl of protein A/G PLUS-Agarose beads (Santa Cruz, sc-2003) were added, and incubated for additional 1 h at 4°C. Beads were pelleted by centrifugation at 2,500 rpm for 5 min at 4°C. The precipitated protein complex was washed with PBS-Tween20 (0.1%) three times and then denatured with 2 X SDS-PAGE loading buffer at 95°C for 8 min. Mammalian cells were lysed in RIPA buffer supplemented with protein protease and phosphatase inhibitors. Protein concentrations were measured with the microplate spectrophotometer Benchmark Plus using protein assay dye (Bio-Rad, 5000006). 10–12% SDS-PAGE was applied to separate the precipitated protein complex or cell lysate, and proteins were transferred to nitrocellulose membranes (0.45 μM). The membrane was blocked with 5% BSA in TBS for 30 min before incubating with primary antibody overnight at 4°C. After washing with TBS-Tween20 (0.1%) three times, the membrane was incubated with the secondary antibody at room temperature for an additional 1 h. The signal was detected with a chemiluminescence imaging system with a CCD camera (LI-COR Biosciences, Odyssey). Western blot data are representative of at least three independent experiments.

Flow cytometry analysis of single cells obtained from tumor tissues—5×10^5 MC38 cells were subcutaneously implanted in the right flanks of adult CDK6 or CDK4 KO mice (male and female) or age-matched wild-type littermates (>6 weeks). Fifteen days after cell injection, tumor tissues were harvested and minced into 1- to 2-mm pieces and digested with 5 mL collagenase Type IV (2 mg/mL) (Gibco, 17104–019) in DMEM for 1 h at 37°C. Cells were collected by centrifugation at 1500 rpm for 10 min and filtered through 70 μm strainers in DMEM media. Cell pellets were suspended in red blood cell lysis buffer (BD, 555899) for 5 min at room temperature. 40 μm strainers were then applied to pass only single cells in PBS supplemented with 2% BSA. Single cells were fixed in 0.5 mL fixation buffer (Biolegend, 420801) in the dark for 20 min at room temperature. Cells were then washed with PBS supplemented with 2% BSA. Cells were stained with corresponding antibodies. The corresponding isotype IgG was applied as a control. Cells were then incubated with antibodies for 30 min at room temperature. Cells were washed with PBS supplemented with 2% BSA and analyzed by flow cytometry. The flow cytometry analysis was performed in the Flow Cytometry and Cell Sorting Shared Resource, Hollings Cancer Center, Medical University of South Carolina (P30 CA138313).

Human T cell isolation and expansion—Primary human peripheral blood recovered from the Leukocyte Reduction System (LRS) cones (Stemcell, 200–0093) was washed with PBS supplemented with 2% FBS in a 50 mL conical tube. An equal volume of Ficoll-Paque PREMIUM (1.084 g/mL) was slowly added to the tube bottom using a 10 mL serological pipette. The mixture was centrifuged at 500 g for 30 min at 22°C with

slow acceleration and brakes turned off. The upper layer of the mixture was removed to a waste bottle, and the layer of monocytes was carefully transferred to a 15 mL conical tube. Monocytes were washed once with EasySep buffer (Stemcell, 20144) once. The EasySep human T cell isolation kit (Stemcell, 17951) was used to isolate T cells from monocytes following the manufacturer's instructions. Isolated T cells were cultured in ImmunoCult-XF T cell expansion medium (Stemcell, 10981) supplemented with human CD3/CD28 T cell Activator (Stemcell, 10971) and human interleukin-2 (10 ng/mL). T cells were expanded in ImmunoCult-XF T cell expansion medium every two days.

OT-I specific TCR transgenic CD8+ T cell activation and expansion—5×10^6 splenocytes from OT-I transgenic mouse spleens per well were plated in a 24-well plate in RPMI-1640 medium containing 10% FBS and supplemented with L-glutamine (2 mM), penicillin (50 U/ml), streptomycin (50 μg/mL) and 2-mercaptoethanol (50 μM). 2 μg/ml OVA peptide dissolved in PBS (OVA 257–264) was added in wells before seeding cells. Following 24 h of incubation, 2 mL fresh medium was added, and cells were divided into 2 wells. 24 h later, 1 mL fresh medium was added to each well, and cells were divided into a new well incubating for another 24 h. At day 3, cells were washed 5 times with PBS and transferred into recipient mice.

For activity measurement, 2×10^6 OVA peptide-activated T cells per well were seeded in a 24-well plate, and cells were treated with inhibitors for LCK kinase (10 μM PP2) or PTP1B/TCPTP (1 μM PTPIB-IN2) for 4 h.

Murine memory T cell differentiation *in vitro*—Murine memory T cell differentiation was performed by adapting the procedures described in a previous study.[94] In brief, a cell suspension of splenocytes from an OT-I CD8 TCR transgenic mouse was plated (day 0) at 5×10^6 per well in T cell media (RPMI-1640 medium containing 10% FBS supplemented with 2 mM L-glutamine, 50 U/ml penicillin, 50 μg/mL streptomycin, and 50 μM 2-mercaptoethanol) with the presence of OVA 257–264 synthetic peptide (1uM), and incubated in the 5% CO_2 at 37°C for 2 h. Cells were spun down at 500 g for 5 min and washed once with T cell media. Cells were resuspended in T cell media, plated at 1 mL/well in a 24-well plate, and incubated for 2 days. Cells were harvested and resuspended in 5 mL T cell media. 2.5 mL Ficoll-Paque PREMIUM (1.084 g/ml) was loaded and spun down at 500 g for 30 min. The cells at the interface were transferred to a new 15 mL conical tube and washed once with T cell media. Cells were resuspended in T cell media containing mouse IL15 (20 ng/mL) and cultured for 2 days. Cells were stained with anti-CD44 and CD62L antibodies for 30 min on ice, then washed with staining buffer twice before flow cytometry analysis.

***In vitro* cell killing assay—**Splenic CD8+ T cells isolated from OT-I mice were pre-activated with OVA peptides for three days. 5×10^5 activated OT-I CD8+ T cells and 1×10^5 MC38-OVA or B16F10-OVA cells (5:1 ratio of T cells: tumor cells) were co-cultured in medium (RPMI supplemented with 10% FBS and 50 μM 2-mercaptoethanol) for 3–5 h in the presence or absence of indicated compounds. Cell mixtures were then collected for flow cytometry analysis. The apoptotic tumor cells were quantified by annexin V/PI staining with flow cytometry. Only tumor cells (CD8-) were quantified.

FACS analysis of cell cycle using BrdU/PI labeling—5-Bromo-2′-deoxyuridine (BrdU) (75 μM) was added to the cell culture medium and incubated for 1 h. Cells were pelleted at 1500 rpm for 5 min and washed with cold PBS. After supernatant removal, cells were resuspended on ice in 200 μL cold PBS. The cells were fixed by adding 5 mL of ice-cold ethanol dropwise and incubated at 4°C overnight. The fixed cells were spun down for 5 min, washed once with PBS, and incubated with 0.5 mL 2 N HCl/0.5% Triton X-100 at room temperature for 30 min to denature the DNA. After adding 5 mL PBS the samples were spun down to remove the supernatant, and the cells were resuspended in 1 mL of $Na_2B_4O_7$, pH 8.5 for neutralization. The cells were spun down, and the supernatant was removed. The cells were then resuspended in 200 μL of anti-BrdU antibodies (BD Biosciences, 556028) diluted in PBS supplemented with 0.5% Tween 20 and 1% BSA at room temperature for 30 min 5 mL of 20 mM HEPES-PBS supplemented with 0.5% Tween 20 was added, and centrifugation was applied to remove the supernatant. The cells were resuspended in 0.5 mL of PBS containing 5 μg/mL propidium iodide (PI) and 200 μg/mL Rnase A. After incubating at room temperature for 30 min, samples were analyzed by flow cytometry.

CD19 CAR T generation—We utilized a CD19-CD28 CAR T construct with CD34-truncated tag (CD34t), obtained from Dr. Michael Nishimura (Loyola) which allowed for the selection of a more purified product with the goal of improving antigen reactivity (i.e., efficacy) and persistence of the cellular product.[95] This construct is also being used to treat CD19+ NHL patients (NCT04214886). Briefly, human PBMCs were TCR activated with anti-CD3 (30 ng/mL) and rhIL-2 (300 IU/mL). After 72 h, T cells were transduced with the retroviral supernatant generated earlier using HEK-293 cells and the modified CD19-CAR construct described earlier.[96] The T cells were then transferred to a G-Rex 10 flask and expanded in G-Rex 10 for 2 days with 300 IU/mL of rhIL2. After 2 days, the transduced T cells were purified using anti-CD34 antibody-coated magnetic beads to obtain a greater than 90% pure population. The purified CD19-CAR T cells were then transferred to a G-Rex 100 flask and expanded in 300 IU/mL of rhIL2 for 7 days to generate a maximum number of purified CD34-expressing CD19-CAR T cells. Cell number and volume were monitored every alternate day with media changes occurring approximately every 3 days. The expanded transduced T cells were cryopreserved at day 12 for experimental use.

CAR T killing assay—For the tumor-killing assay, Raji cells (2×10^4) expressing CD19 and GFP were co-cultured with CD19 CAR T cells (2×10^5; Raji:T cell ratio 1:10) for 16 h in IMDM media supplemented with 10% FBS. The co-cultured cells were treated with either CDK6 degrader, PTPs inhibitor or vehicle. Cells were then incubated with mAb against human CD8, CD34, annexin V, and 7-AAD. Cytotoxicity was determined by the percentage of apoptotic (annexin V+7-AAD+) Raji cells. T cells without CAR expression co-cultured with Raji cells under degrader/inhibitor/vehicle treatment were used as controls. For PTPs inhibition, PTP1B-IN2 was applied to treat CAR T cells 10 min early before co-culturing with Raji cells.

Recombinant PTPs protein expression and purification—Expression and purification of recombinant protein were performed as described in our previous work.[30]

In brief, E. coli BL21 was used for recombinant protein expression. BL21 was inoculated in autoclaved Luria Broth (LB) medium (1% bacto-tryptone, 0.5% bacto-yeast-extract and 1% NaCl) supplemented with ampicillin or kanamycin (50 μg/mL). BL21 was cultured in LB medium shaking at 220 rpm at 37°C until OD600nm reached 0.4 to 0.6. Isopropyl-β-D-thiogalactoside (IPTG) was added to the LB medium to a final concentration of 0.2 μM to induce recombinant protein expression. Bacteria were collected 6 h later with centrifuging at 6,000 rpm at 4°C for 10 min. The pellet was washed with cold PBS twice and then lysed in lysis buffer (20 mM Tris-HCl, pH 8.0; 2 μM EDTA; 1% Triton X-100) containing 1 mg/mL lysozyme. The lysate was sonicated for 90 s on ice and centrifuged at 17,000 rpm for 20 min. The lysates were used to purify PTP1B and TCPTP. Glutathione Sepharose was used to purify GST-tagged PTP1B. Ni-NTA agarose was applied to purify HIS-tagged TCPTP.

***In vitro* cyclin D2/3-CDK4/6 kinase assay—**Kinase assays were performed in 30 μL of kinase buffer as described previously[30]: 50 mM HEPES (pH 7.5), 10 mM $MgCl_2$, 1 mM dithiothreitol (DTT), 1 mM EGTA, 0.1 mM NaF, containing 10 μM ATP. 0.2 μg of cyclin D2–CDK6, cyclin D3–CDK4, cyclin D2–CDK4 or cyclin D3–CDK6 were used as kinases. Recombinant PTP1B or TCPTP protein (commercial or homemade) were used as kinase substrates. Recombinant human PTP1B (1366-PT-050) and TCPTP (1930-PT-050) were purchased from R&D. 0.1 μg of recombinant Rb C-terminal protein (Santa Cruz, sc-4112) was used as a positive control. 2 μg of BSA was used as a negative control. After incubation at 30°C for 30 min, proteins were denatured at 95°C for 8 min, resolved on SDS–PAGE, and transferred to nitrocellulose membranes and followed for immunoblotting using specific phosphorylation antibodies.

Phosphatase assay—Recombinant PTP proteins (PTP1B and TCPTP) phosphorylated by cyclin D3/CDK6 kinase or PTPs immunoprecipitated from Jurkat cell lysates were applied to measure their phosphatase activities. Tyrosine phosphatase substrate I, DADEY(PO3)LIPQQG (R&D, ES006), or phosphorylated CD3ζ (p-CD3ζ) by LCK kinase was used as substrates. Phosphatase assay buffer: 10mM HEPES, 0.1mM EDTA, 0.1mM EGTA, 0.2 mg/mL BSA, 1mM dithiothreitol, pH 7.5. 0.1 or 0.5 μg of recombinant proteins were used. Phosphatase assays were followed with Malachite Green Phosphate Detection Kit (R&D, DY996). Phosphatase activity (μmol/min/mg) was calculated as [Phosphate released (nmol) X (0.001 μMol/1 nmol)]/[incubation time (min) X amount of enzyme (mg)].

Tandem mass Tag-MS analysis of KOPTK1 cells treated with CDK4/6 inhibitors

Identification of substrates using the inhibition approach: KOPTK1 cells were cultured in RPMI 1640 medium without feeders. Five plates were cultured for 8 h with 1 μM palbociclib and the other five were treated with an equal volume of DMSO. The cells were washed with ice-cold PBS and cells from each plate were harvested separately in 5 mL of 2% SDS in 50 mM Tris (pH 8.5) with Halt protease and phosphatase inhibitors (Pierce). The lysates were flash frozen in liquid nitrogen and stored frozen until analysis by tandem mass spectrometry.

Lysis and protein digestion: Each sample was lysed in 8 M urea in 50 mM Tris with Halt protease and phosphatase inhibitors. Samples were reduced with 5 mM dithiouritol for 30

min at room temperature followed by alkylation with 25 mM iodoacetamide for 30 min at room temperature in the dark. Samples were then methanol/chloroform precipitated using a 4:4:1 ratio of methanol to sample to chloroform. Pellets after precipitation were resuspended in 2 M urea with 50 mM TRIS (pH 8.5) and digested with Lys-C (100:1 protein:enzyme) overnight at 37°C followed by trypsin digestion (100:1 protein:enzyme) at 37°C for 4 h. Peptides were desalted using 500 mg Sep-Pak desalting cartridges and dried overnight.

Phosphopeptide enrichment: Digested peptides (~10 mg per TMT channel) were resuspended in 1 mL of 2 M lactic acid/50% acetonitrile (ACN) and centrifuged at 15000 g for 20 min. Supernatants were removed, placed in an Eppendorf tube containing 15 mg of titanium dioxide beads (GL Sciences, Japan), and vortexed for 1 h at room temperature. Beads were washed twice with 2 M lactic acid/50% ACN and once with 0.1% TFA in 50% ACN. Phosphopeptides were eluted twice with 150 μL of 50 mM dipotassium phosphate, pH 10, acidified with 40 μL of 20% formic acid, and subjected to C18 StageTip desalting (3M Empore, South Eagan, MN).

TMT labeling: Isobaric labeling of the enriched phosphopeptides was performed using 10-plex tandem mass tag (TMT) reagents (Thermo Fisher Scientific, Rockford, IL). TMT reagents (5 mg) were dissolved in 250 μL of dry acetonitrile (ACN), and 10 μL was added to 100 μg (quantified by Micro BCA, Thermo Scientific, Rockford, IL) of phosphopeptides dissolved in 100 μL of 200 mM HEPES (pH 8.5). After 1 h, the reaction was quenched by adding 8 μL of 5% hydroxylamine. Labeled peptides were combined, acidified with 20 μL of 20% FA (pH ~2), and concentrated *via* C18 SPE on Sep-Pak cartridges (50 mg bed volume).

Basic pH reverse phase liquid chromatography: TMT-labeled phosphopeptides were subjected to orthogonal basic-pH reverse phase (bpHrp) fractionation. Labeled phosphopeptides were solubilized in buffer A (5% ACN, 10 mM ammonium bicarbonate, pH 8.0) and separated on an Agilent 300 Extend C18 column (5 μm particles, 4.6 mm i.d. and 220 mm length). Using an Agilent 1100 binary pump equipped with a degasser and a photodiode array (PDA) detector (Thermo Scientific, San Jose, CA), a 45 min linear gradient from 8% to 35% acetonitrile in 10 mM ammonium bicarbonate (pH 8.0) (flow rate of 0.8 mL/min) separated the peptide mixtures into a total of 96 fractions. The 96 fractions were consolidated into 24 samples in a checkerboard manner, acidified with 10 μL of 20% formic acid, and vacuum dried. Each sample was redissolved in 5% formic acid, desalted *via* StageTip, dried *via* vacuum centrifugation, and reconstituted for LC-MS/MS analysis.

Liquid chromatography electrospray ionization tandem mass spectrometry (LC-ESI-MS/MS) and data analysis: Each LC-MS/MS data collection cycle was performed with one full MS scan (400–1400 m/z) acquired in the Orbitrap (1.2×10^5 resolutions and an AGC of 2×10^5 ions). The subsequent MS2-MS3 analysis was conducted for top 10 most intense ions and fragmented by CID with the following settings: collision energy of 35%, AGC 4×10^3, isolation window 0.5 Da, maximum ion accumulation time 150 ms with 40 s of dynamic exclusion. Following the MS2 scan, for the MS3 analyses, precursor isolation was performed using a 2.5 Da window and fragmented in the ion trap using CID using a collision energy of 35%, AGC targeted of 8,000 ions and a maximum ion

injection time of 150 ms. Multiple fragment ions (SPS ions) were co-isolated and further fragmented by HCD. Selection of fragment ions was based on the previous MS2 scan and the MS2-MS3 was conducted using a recently described sequential precursor selection (SPS) methodology.[97] MS3 was performed using HCD with 55% collision energy and reporter ion detection in the Orbitrap with an AGC of 150,000 ions, a resolution of 60,000 and a maximum ion accumulation time of 150 ms.

Database searching and reporter ion quantitation in-house software tools were used to convert the RAW file to the.mzxml format.[98] Correction of erroneous charge state and monoisotopic m/z values were performed using the method detailed in.[98] Assignment of MS/MS spectra was made with the Sequest algorithm[99] using an indexed Uniprot mouse database (compiled 2016) prepared with forward and reverse sequences concatenated per the target-decoy strategy.[100] Database searches were conducted using cysteine alkylation and TMT on the peptide N-termini and lysine residues as static modification, oxidation of methionine as a dynamic modification, precursor ion tolerance of 20 ppm and a fragment ion tolerance of 0.8 Da (for CID). Sequest matches were filtered using linear discriminant analysis as previously reported[100] first to a dataset level error of 1% at the peptide level based on matches to reversed sequences. Protein rankings were generated by multiplying peptide probabilities, and the dataset was finally filtered to 1% FDR at the protein level. The final peptide-level FDR fell well below 1% (~0.2% peptide level). A reductionist model was used for the assignment of peptides to protein matches, where all peptides were explained using the least number of proteins.

Quantitation of peptides using TMT reporter ions was performed as previously published.[97,101] Briefly, a 0.003 Th window centered on the theoretical m/z value of each reporter ion was recorded for each of the 6 reporter ions, and the intensity of the signal closest to the theoretical m/z value was recorded. TMT signals were also corrected for isotope impurities according to the manufacturer's instructions. Peptides were only considered quantifiable if the total signal-to-noise for all channels was >200 and the isolation specificity was >0.75. Within each TMT experiment, peptide quantitation was normalized by summing the values across each channel and then each channel was corrected so that all channels had the same summed value. Protein quantitation was performed by summing the signal-to-noise for all peptides for a given protein.

Statistical analyses of phosphopeptide site localization and quantitation: We used a modified version of the Ascore algorithm to quantify the confidence with which a phosphorylation site could be assigned to a particular residue. Phosphorylation sites with Ascore values > 13 ($p \leq 0.05$) were considered confidently localized to a particular residue.[98] Student's t-test was used to assign confidence to changes in phosphopeptide abundance. Multiple test correction was performed by adjusting the calculated p values according to Benjamini–Hochberg.

MS following *in vitro* kinase assay to determine protein phosphorylation sites

—Recombinant PTP (PTP1B and TCPTP) proteins were phosphorylated by cyclin D3/CDK6 as described for the kinase assay. Protein mixtures were separated by SDS-PAGE followed by Coomassie Blue staining. Recombinant PTPs without phosphorylation were

used as controls. PTP protein bands were excised from SDS-PAGE gels and cut into 1 mm2 pieces. After de-staining, the PTP1B and TCPTP protein bands were reduced with dithiothreitol (DTT) (32 mM DTT; room temperature incubation for 30 min), alkylated with iodoacetamide (IAA) (80mM IAA; room temperature for 30 min in the dark), and digested with porcine trypsin (in 50 mM ammonium bicarbonate; 37°C; overnight). Peptides were released from the gels using a sequential extraction with 50% acetonitrile (ACN)/5% formic acid (FA) followed by 85% ACN/5% FA. The extracted peptides were dried using a vacuum centrifuge. Samples were then desalted using C18 Stage tips (Thermo Scientific), and the eluates were dried by vacuum centrifugation. The eluates were redissolved in 2% ACN/ 0.1% FA and injected into an Orbitrap Fusion Lumos mass spectrometer equipped with an Easy-nLC 1200 HPLC system (Thermo Scientific). The peptides were separated using an Acclaim PepMap RSLC column (75 μm × 50 cm, C18, 2 μm, 100 Å at 45°C). A 180 min gradient from 2% B to 35% B was used (Solvent A = 2% ACN/0.1% FA – Solvent B = 80% ACN/0.1% FA). MS1 scans were detected in the Orbitrap at 60,000 resolution; MS2 scans were also detected in the Orbitrap at 15,000 resolution. High collision dissociation was used to fragment the selected precursors (35% collision). The data dependent acquisition cycle time was 3 s. Dynamic exclusion was implemented. The raw data files were searched using Proteome Discoverer 1.4 (Thermo Scientific) and BioPharma Finder v2.0.1.0 (Thermo Scientific) against a database containing the sequence of the proteins of interest, trypsin as enzyme, oxidation (M) and phosphorylation (S, T, Y) as variable modifications, and carbamidomethyl (C) as fixed modification. The search results were filtered to include only highly confidently identified peptides. The phosphorylated peptide spectra were manually inspected.

Bioinformatic analysis—The association between Cyclin D/CDK expression and Progression-Free Survival (PFS) of melanoma patients receiving single-agent immunotherapy treatment was tested by the two-sided Wald test in a Cox-PH regression. Data from single agent immunotherapy (anti-CTLA4 or anti-PD1 or adoptive T cell therapy (ACT)) were analyzed using Kaplan-Meier plots comparing patients with top CDK6 (CDK6 high, above average) and bottom CDK6 (CDK6 low, below average) expression levels. The average of all samples in each study was used as the normalization control for each gene. The clinical studies with single-agent immunotherapy and patient numbers over 20 were chosen. Data were derived from http://tide.dfci.harvard.edu.[38,102] In Figure 1A, A positive score (red) indicates a positive correlation between CDK6 expression level and risk of death (reflected by PFS on anti-PD1Ab, anti-CTLA4 Ab, or ACT immunotherapy treatment). A negative score (blue) denotes a negative correlation. CCND1: cyclin D1; CCND2: cyclin D2; CCND3: cyclin D3. Naive: patients naive to PD-1 Abs; Prog: patients who had previous treatment with PD-1 Abs.

TIMER web server (https://cistrome.shinyapps.io/timer/) was applied to systematically analyze immune infiltrates across metastatic skin cutaneous melanoma. The original source data was from TCGA data portal (https://gdc.nci.nih.gov) and GDAC Firehose website (http://gdac.broadinstitute.org). The Gene module was applied to visualize the correlation of its expression with immune infiltration level in melanoma. Genes highly expressed in the

microenvironment are expected to have negative associations with tumor purity, while the opposite is expected for genes highly expressed in the tumor cells.

QUANTIFICATION AND STATISTICAL ANALYSIS

GraphPad Prism 9 was used for data analysis and statistical significance was calculated using the unpaired, two-tailed Student's t-test or 1-way ANOVA. Survival in mouse experiments was represented with Kaplan-Meier curves and the log rank test was applied for statistical survival analysis. Analyses were not performed under specific randomization or blinding protocol. Statistically significant differences are indicated in figures with the accompanying p value in the legend. Error bars in figures indicate the standard error of the mean (SEM) for the number of animals or replicates, as indicated in the figure legend. $p < 0.05$ (*), $p < 0.01$ (**), $p < 0.001$ (***), and $p < 0.0001$ (****) were considered significant.

Supplementary Material

Refer to Web version on PubMed Central for supplementary material.

ACKNOWLEDGMENTS

We thank Mariano Barbacid for sharing CDK6 knockout mice and Hiroaki Kiyokawa for CDK4 knockout mice. This work was supported by the American Cancer Society Institutional Research (IRG-19-137-20 to X.G.), the SC COBRE in Oxidants, Redox Balance and Stress Signaling Pilot Projects Program (1P30CM140964 to X.G.), the National Institute of General Medical Sciences Pilot Project (P20GM130457 to X.G.), the Leukemia Research Foundation (to M.I.N.), the National Institutes of Health (R37CA251165 to H.W., R01CA236226 to P.S., and R01HL140953, R21 CA263140, and R01 CA258440 to X.-Z.Y.), the SC SmartState Cancer Stem Cell Biology & Therapy Program (to X.-Z.Y.), and the Bristol-Myers Squibb Melanoma Research Alliance Young Investigator Award (821901 to H.W.).

REFERENCES

1. Sharma P, Hu-Lieskovan S, Wargo JA, and Ribas A. (2017). Primary, adaptive, and acquired resistance to cancer immunotherapy. Cell 168, 707–723. 10.1016/j.cell.2017.01.017. [PubMed: 28187290]
2. Yu Q, Geng Y, and Sicinski P. (2001). Specific protection against breast cancers by cyclin D1 ablation. Nature 411, 1017–1021. 10.1038/35082500. [PubMed: 11429595]
3. Yu Q, Sicinska E, Geng Y, Ahnström M, Zagozdzon A, Kong Y, Gardner H, Kiyokawa H, Harris LN, Stål O, and Sicinski P. (2006). Requirement for CDK4 kinase function in breast cancer. Cancer Cell 9, 23–32. 10.1016/j.ccr.2005.12.012. [PubMed: 16413469]
4. Boonen GJ, van Oirschot BA, van Diepen A, Mackus WJ, Verdonck LF, Rijksen G, and Medema RH (1999). Cyclin D3 regulates proliferation and apoptosis of leukemic T cell lines. J. Biol. Chem 274, 34676–34682. [PubMed: 10574933]
5. Choi YJ, Li X, Hydbring P, Sanda T, Stefano J, Christie AL, Signoretti S, Look AT, Kung AL, von Boehmer H, and Sicinski P. (2012). The requirement for cyclin D function in tumor maintenance. Cancer Cell 22, 438–451. 10.1016/j.ccr.2012.09.015. [PubMed: 23079655]
6. Malumbres M, Sotillo R, Santamaría D, Galán J, Cerezo A, Ortega S, Dubus P, and Barbacid M. (2004). Mammalian cells cycle without the D-type cyclin-dependent kinases Cdk4 and Cdk6. Cell 118, 493–504. 10.1016/j.cell.2004.08.002. [PubMed: 15315761]
7. DeMichele A, Clark AS, Tan KS, Heitjan DF, Gramlich K, Gallagher M, Lal P, Feldman M, Zhang P, Colameco C, et al. (2015). CDK 4/6 inhibitor palbociclib (PD0332991) in Rb+ advanced breast cancer: phase II activity, safety, and predictive biomarker assessment. Clin. Cancer Res 21, 995–1001. 10.1158/1078-0432.CCR-14-2258. [PubMed: 25501126]

8. Lu J. (2015). Palbociclib: a first-in-class CDK4/CDK6 inhibitor for the treatment of hormone-receptor positive advanced breast cancer. J. Hematol. Oncol 8, 98. 10.1186/s13045-015-0194-5. [PubMed: 26264704]
9. Turner NC, Ro J, André F, Loi S, Verma S, Iwata H, Harbeck N, Loibl S, Huang Bartlett C, Zhang K, et al. (2015). Palbociclib in hormone-receptor-positive advanced breast cancer. N. Engl. J. Med 373, 209–219. 10.1056/NEJMoa1505270. [PubMed: 26030518]
10. Vaughn DJ, Hwang WT, Lal P, Rosen MA, Gallagher M, and O'Dwyer PJ (2015). Phase 2 trial of the cyclin-dependent kinase 4/6 inhibitor palbociclib in patients with retinoblastoma protein-expressing germ cell tumors. Cancer 121, 1463–1468. 10.1002/cncr.29213. [PubMed: 25522918]
11. Cristofanilli M, Turner NC, Bondarenko I, Ro J, Im SA, Masuda N, Colleoni M, DeMichele A, Loi S, Verma S, et al. (2016). Fulvestrant plus palbociclib versus fulvestrant plus placebo for treatment of hormone-receptor-positive, HER2-negative metastatic breast cancer that progressed on previous endocrine therapy (PALOMA-3): final analysis of the multicentre, double-blind, phase 3 randomised controlled trial. Lancet Oncol. 17, 425–439. 10.1016/S1470-2045(15)00613-0. [PubMed: 26947331]
12. Finn RS, Martin M, Rugo HS, Jones S, Im SA, Gelmon K, Harbeck N, Lipatov ON, Walshe JM, Moulder S, et al. (2016). Palbociclib and letrozole in advanced breast cancer. N. Engl. J. Med 375, 1925–1936. 10.1056/NEJMoa1607303. [PubMed: 27959613]
13. Finn RS, Crown JP, Ettl J, Schmidt M, Bondarenko IM, Lang I, Pinter T, Boer K, Patel R, Randolph S, et al. (2016). Efficacy and safety of palbociclib in combination with letrozole as first-line treatment of ER-positive, HER2-negative, advanced breast cancer: expanded analyses of subgroups from the randomized pivotal trial PALOMA-1/TRIO-18. Breast Cancer Res. 18, 67. 10.1186/s13058-016-0721-5. [PubMed: 27349747]
14. Sherr CJ, Beach D, and Shapiro GI (2016). Targeting CDK4 and CDK6: from discovery to therapy. Cancer Discov. 6, 353–367. 10.1158/2159-8290.CD-15-0894. [PubMed: 26658964]
15. Tamura K, Mukai H, Naito Y, Yonemori K, Kodaira M, Tanabe Y, Yamamoto N, Osera S, Sasaki M, Mori Y, et al. (2016). Phase I study of palbociclib, a cyclin-dependent kinase 4/6 inhibitor, in Japanese patients. Cancer Sci. 107, 755–763. 10.1111/cas.12932. [PubMed: 26991823]
16. Lynce F, Saleh M, Shajahan-Haq A, Gallagher C, Dilawari A, Hahn O, Abu-Khalaf M, Cai L, Pohlmann P, Mohebtash M, et al. (2018). PALINA: a phase II safety study of palbociclib in combination with letrozole or fulvestrant in African American women with hormone receptor positive HER2 negative advanced breast cancer. Contemp. Clin. Trials Commun. 10, 190–192. 10.1016/j.conctc.2018.05.012. [PubMed: 30009277]
17. Taylor JW, Parikh M, Phillips JJ, James CD, Molinaro AM, Butowski NA, Clarke JL, Oberheim-Bush NA, Chang SM, Berger MS, and Prados M. (2018). Phase-2 trial of palbociclib in adult patients with recurrent RB1-positive glioblastoma. J. Neuro Oncol 140, 477–483. 10.1007/s11060-018-2977-3.
18. Turner NC, Slamon DJ, Ro J, Bondarenko I, Im SA, Masuda N, Colleoni M, DeMichele A, Loi S, Verma S, et al. (2018). Overall survival with palbociclib and fulvestrant in advanced breast cancer. N. Engl. J. Med 379, 1926–1936. 10.1056/NEJMoa1810527. [PubMed: 30345905]
19. Masuda N, Inoue K, Nakamura R, Rai Y, Mukai H, Ohno S, Hara F, Mori Y, Hashigaki S, Muramatsu Y, et al. (2019). Palbociclib in combination with fulvestrant in patients with hormone receptor-positive, human epidermal growth factor receptor 2-negative advanced breast cancer: PALOMA-3 subgroup analysis of Japanese patients. Int. J. Clin. Oncol 24, 262–273. 10.1007/s10147-018-1359-3. [PubMed: 30392115]
20. Yang L, Xue J, Yang Z, Wang M, Yang P, Dong Y, He X, Bao G, and Peng S. (2021). Side effects of CDK4/6 inhibitors in the treatment of HR+/HER2− advanced breast cancer: a systematic review and meta-analysis of randomized controlled trials. Ann. Palliat. Med 10, 5590–5599. 10.21037/apm-21-1096. [PubMed: 34107710]
21. Jazieh KA, Budd GT, Dalpiaz N, and Abraham J. (2019). Can CDK4/6 inhibitors cause fatal lung injury? Expert Rev. Anticancer Ther. 19, 917–919. 10.1080/14737140.2019.1674651.
22. Thill M, and Schmidt M. (2018). Management of adverse events during cyclin-dependent kinase 4/6 (CDK4/6) inhibitor-based treatment in breast cancer. Ther. Adv. Med. Oncol 10, 1758835918793326. 10.1177/1758835918793326.

23. O'Leary B, Cutts RJ, Liu Y, Hrebien S, Huang X, Fenwick K, André F, Loibl S, Loi S, Garcia-Murillas I, et al. (2018). The genetic land-scape and clonal evolution of breast cancer resistance to palbociclib plus fulvestrant in the PALOMA-3 trial. Cancer Discov. 8, 1390–1403. 10.1158/2159-8290.CD-18-0264. [PubMed: 30206110]
24. Hortobagyi GN, Stemmer SM, Burris HA, Yap YS, Sonke GS, Paluch-Shimon S, Campone M, Petrakova K, Blackwell KL, Winer EP, et al. (2018). Updated results from MONALEESA-2, a phase III trial of first-line ribociclib plus letrozole versus placebo plus letrozole in hormone receptor-positive, HER2-negative advanced breast cancer. Ann. Oncol 29, 1541–1547. 10.1093/annonc/mdy155. [PubMed: 29718092]
25. Gong J, Cho M, Yu KW, Waisman J, Yuan Y, and Mortimer J. (2018). A single institution experience with palbociclib toxicity requiring dose modifications. Breast Cancer Res. Treat 168, 381–387. 10.1007/s10549-017-4606-9. [PubMed: 29218462]
26. Dickler MN, Tolaney SM, Rugo HS, Cortés J, Diéras V, Patt D, Wildiers H, Hudis CA, O'Shaughnessy J, Zamora E, et al. (2017). MONARCH 1, A phase II study of abemaciclib, a CDK4 and CDK6 inhibitor, as a single agent, in patients with refractory HR(+)/HER2(−) metastatic breast cancer. Clin. Cancer Res 23, 5218–5224. 10.1158/1078-0432.CCR-17-0754. [PubMed: 28533223]
27. Herrera-Abreu MT, Palafox M, Asghar U, Rivas MA, Cutts RJ, Garcia-Murillas I, Pearson A, Guzman M, Rodriguez O, Grueso J, et al. (2016). Early adaptation and acquired resistance to CDK4/6 inhibition in estrogen receptor-positive breast cancer. Cancer Res. 76, 2301–2313. 10.1158/0008-5472.CAN-15-0728. [PubMed: 27020857]
28. Gao X, Qin S, Wu Y, Chu C, Jiang B, Johnson RH, Kuang D, Zhang J, Wang X, Mehta A, et al. (2021). Nuclear PFKP promotes CXCR4-dependent infiltration by T cell acute lymphoblastic leukemia. J. Clin. Invest 131, e143119. 10.1172/JCI143119. [PubMed: 34255748]
29. Zhang J, Bu X, Wang H, Zhu Y, Geng Y, Nihira NT, Tan Y, Ci Y, Wu F, Dai X, et al. (2018). Cyclin D-CDK4 kinase destabilizes PD-L1 via cullin 3-SPOP to control cancer immune surveillance. Nature 553, 91–95. 10.1038/nature25015. [PubMed: 29160310]
30. Wang H, Nicolay BN, Chick JM, Gao X, Geng Y, Ren H, Gao H, Yang G, Williams JA, Suski JM, et al. (2017). The metabolic function of cyclin D3-CDK6 kinase in cancer cell survival. Nature 546, 426–430. 10.1038/nature22797. [PubMed: 28607489]
31. Hanahan D, and Coussens LM (2012). Accessories to the crime: functions of cells recruited to the tumor microenvironment. Cancer Cell 21, 309–322. 10.1016/j.ccr.2012.02.022. [PubMed: 22439926]
32. Quail DF, and Joyce JA (2013). Microenvironmental regulation of tumor progression and metastasis. Nat. Med 19, 1423–1437. 10.1038/nm.3394. [PubMed: 24202395]
33. Borst J, Ahrends T, Bąbała N, Melief CJM, and Kastenmüller W. (2018). CD4(+) T cell help in cancer immunology and immunotherapy. Nat. Rev. Immunol 18, 635–647. 10.1038/s41577-018-0044-0. [PubMed: 30057419]
34. Lin J, and Weiss A. (2001). T cell receptor signalling. J. Cell Sci 114, 243–244. [PubMed: 11148124]
35. Yudushkin IA, and Vale RD (2010). Imaging T-cell receptor activation reveals accumulation of tyrosine-phosphorylated CD3ζeta in the endosomal compartment. Proc. Natl. Acad. Sci. USA 107, 22128–22133. 10.1073/pnas.1016388108. [PubMed: 21135224]
36. Guy CS, Vignali KM, Temirov J, Bettini ML, Overacre AE, Smeltzer M, Zhang H, Huppa JB, Tsai YH, Lobry C, et al. (2013). Distinct TCR signaling pathways drive proliferation and cytokine production in T cells. Nat. Immunol 14, 262–270. 10.1038/ni.2538. [PubMed: 23377202]
37. Wiede F, Shields BJ, Chew SH, Kyparissoudis K, van Vliet C, Galic S, Tremblay ML, Russell SM, Godfrey DI, and Tiganis T. (2011). T cell protein tyrosine phosphatase attenuates T cell signaling to maintain tolerance in mice. J. Clin. Invest 121, 4758–4774. 10.1172/JCI59492. [PubMed: 22080863]
38. Jiang P, Gu S, Pan D, Fu J, Sahu A, Hu X, Li Z, Traugh N, Bu X, Li B, et al. (2018). Signatures of T cell dysfunction and exclusion predict cancer immunotherapy response. Nat. Med 24, 1550–1558. 10.1038/s41591-018-0136-1. [PubMed: 30127393]

39. Liu D, Schilling B, Liu D, Sucker A, Livingstone E, Jerby-Arnon L, Zimmer L, Gutzmer R, Satzger I, Loquai C, et al. (2019). Integrative molecular and clinical modeling of clinical outcomes to PD1 blockade in patients with metastatic melanoma. Nat. Med 25, 1916–1927. 10.1038/s41591-019-0654-5. [PubMed: 31792460]
40. Li T, Fu J, Zeng Z, Cohen D, Li J, Chen Q, Li B, and Liu XS (2020). TIMER2.0 for analysis of tumor-infiltrating immune cells. Nucleic Acids Res. 48, W509–W514. 10.1093/nar/gkaa407. [PubMed: 32442275]
41. Chinnaiyan AM, Hanna WL, Orth K, Duan H, Poirier GG, Froelich CJ, and Dixit VM (1996). Cytotoxic T-cell-derived granzyme B activates the apoptotic protease ICE-LAP3. Curr. Biol 6, 897–899. 10.1016/s0960-9822(02)00614-0. [PubMed: 8805307]
42. Ghanekar SA, Nomura LE, Suni MA, Picker LJ, Maecker HT, and Maino VC (2001). Gamma interferon expression in CD8(+) T cells is a marker for circulating cytotoxic T lymphocytes that recognize an HLA A2-restricted epitope of human cytomegalovirus phosphoprotein pp65. Clin. Diagn. Lab. Immunol 8, 628–631. 10.1128/CDLI.8.3.628-631.2001. [PubMed: 11329470]
43. Ostroumov D, Fekete-Drimusz N, Saborowski M, Kühnel F, and Woller N. (2018). CD4 and CD8 T lymphocyte interplay in controlling tumor growth. Cell. Mol. Life Sci 75, 689–713. 10.1007/s00018-017-2686-7. [PubMed: 29032503]
44. Reiser J, and Banerjee A. (2016). Effector, memory, and dysfunctional CD8(+) T cell fates in the antitumor immune response. J. Immunol. Res 2016, 8941260. 10.1155/2016/8941260. [PubMed: 27314056]
45. Crouse J, Xu HC, Lang PA, and Oxenius A. (2015). NK cells regulating T cell responses: mechanisms and outcome. Trends Immunol. 36, 49–58. 10.1016/j.it.2014.11.001. [PubMed: 25432489]
46. Krebs P, Barnes MJ, Lampe K, Whitley K, Bahjat KS, Beutler B, Janssen E, and Hoebe K. (2009). NK-cell-mediated killing of target cells triggers robust antigen-specific T-cell-mediated and humoral responses. Blood 113, 6593–6602. 10.1182/blood-2009-01-201467. [PubMed: 19406986]
47. Mocikat R, Braumüller H, Gumy A, Egeter O, Ziegler H, Reusch U, Bubeck A, Louis J, Mailhammer R, Riethmüller G, et al. (2003). Natural killer cells activated by MHC class I(low) targets prime dendritic cells to induce protective CD8 T cell responses. Immunity 19, 561–569. 10.1016/s1074-7613(03)00264-4. [PubMed: 14563320]
48. Gerosa F, Baldani-Guerra B, Nisii C, Marchesini V, Carra G, and Trinchieri G. (2002). Reciprocal activating interaction between natural killer cells and dendritic cells. J. Exp. Med 195, 327–333. 10.1084/jem.20010938. [PubMed: 11828007]
49. Zamai L, Ponti C, Mirandola P, Gobbi G, Papa S, Galeotti L, Cocco L, and Vitale M. (2007). NK cells and cancer. J. Immunol 178, 4011–4016. 10.4049/jimmunol.178.7.4011. [PubMed: 17371953]
50. Klein K, Witalisz-Siepracka A, Gotthardt D, Agerer B, Locker F, Grausenburger R, Knab VM, Bergthaler A, and Sexl V. (2021). T cell-intrinsic CDK6 is dispensable for anti-viral and anti-tumor responses in vivo. Front. Immunol 12, 650977. 10.3389/fimmu.2021.650977. [PubMed: 34248938]
51. Muranski P, Boni A, Antony PA, Cassard L, Irvine KR, Kaiser A, Paulos CM, Palmer DC, Touloukian CE, Ptak K, et al. (2008). Tumor-specific Th17-polarized cells eradicate large established melanoma. Blood 112, 362–373. 10.1182/blood-2007-11-120998. [PubMed: 18354038]
52. . Ochsenbein AF (2005). Immunological ignorance of solid tumors. Springer Semin. Immunopathol. 27, 19–35. 10.1007/s00281-004-0192-0.
53. Overwijk WW, Theoret MR, Finkelstein SE, Surman DR, de Jong LA, Vyth-Dreese FA, Dellemijn TA, Antony PA, Spiess PJ, Palmer DC, et al. (2003). Tumor regression and autoimmunity after reversal of a functionally tolerant state of self-reactive CD8+ T cells. J. Exp. Med 198, 569–580. 10.1084/jem.20030590. [PubMed: 12925674]
54. Ochsenbein AF, Klenerman P, Karrer U, Ludewig B, Pericin M, Hengartner H, and Zinkernagel RM (1999). Immune surveillance against a solid tumor fails because of immunological ignorance. Proc. Natl. Acad. Sci. USA 96, 2233–2238. 10.1073/pnas.96.5.2233. [PubMed: 10051624]

55. Anders L, Ke N, Hydbring P, Choi YJ, Widlund HR, Chick JM, Zhai H, Vidal M, Gygi SP, Braun P, and Sicinski P. (2011). A systematic screen for CDK4/6 substrates links FOXM1 phosphorylation to senescence suppression in cancer cells. Cancer Cell 20, 620–634. 10.1016/j.ccr.2011.10.001. [PubMed: 22094256]
56. Xu Y, and Fisher GJ (2012). Receptor type protein tyrosine phosphatases (RPTPs) - roles in signal transduction and human disease. J. Cell Commun. Signal 6, 125–138. 10.1007/s12079-012-0171-5. [PubMed: 22851429]
57. Bourdeau A, Dubé N, and Tremblay ML (2005). Cytoplasmic protein tyrosine phosphatases, regulation and function: the roles of PTP1B and TC-PTP. Curr. Opin. Cell Biol 17, 203–209. 10.1016/j.ceb.2005.02.001. [PubMed: 15780598]
58. Simoncic PD, McGlade CJ, and Tremblay ML (2006). PTP1B and TC-PTP: novel roles in immune-cell signaling. Can. J. Physiol. Pharmacol 84, 667–675. 10.1139/y06-012. [PubMed: 16998530]
59. Doody KM, Bourdeau A, and Tremblay ML (2009). T-cell protein tyrosine phosphatase is a key regulator in immune cell signaling: lessons from the knockout mouse model and implications in human disease. Immunol. Rev 228, 325–341. 10.1111/j.1600-065X.2008.00743.x. [PubMed: 19290937]
60. Jiang B, Wang ES, Donovan KA, Liang Y, Fischer ES, Zhang T, and Gray NS (2019). Development of dual and selective degraders of cyclin-dependent kinases 4 and 6. Angew. Chem. Int. Ed. Engl 58, 6321–6326. 10.1002/anie.201901336. [PubMed: 30802347]
61. Modiano JF, Mayor J, Ball C, Fuentes MK, and Linthicum DS (2000). CDK4 expression and activity are required for cytokine responsiveness in T cells. J. Immunol 165, 6693–6702. 10.4049/jimmunol.165.12.6693. [PubMed: 11120786]
62. Rossy J, Williamson DJ, and Gaus K. (2012). How does the kinase Lck phosphorylate the T cell receptor? Spatial organization as a regulatory mechanism. Front. Immunol 3, 167. 10.3389/fimmu.2012.00167. [PubMed: 22723799]
63. Nika K, Soldani C, Salek M, Paster W, Gray A, Etzensperger R, Fugger L, Polzella P, Cerundolo V, Dushek O, et al. (2010). Constitutively active Lck kinase in T cells drives antigen receptor signal transduction. Immunity 32, 766–777. 10.1016/j.immuni.2010.05.011. [PubMed: 20541955]
64. Palacios EH, and Weiss A. (2004). Function of the src-family kinases, lck and fyn, in T-cell development and activation. Oncogene 23, 7990–8000. 10.1038/sj.onc.1208074. [PubMed: 15489916]
65. Liu P, Du Y, Song L, Shen J, and Li Q. (2016). Discovery of novel, high potent, ABC type PTP1B inhibitors with TCPTP selectivity and cellular activity. Eur. J. Med. Chem 118, 27–33. 10.1016/j.ejmech.2016.04.014. [PubMed: 27123900]
66. Lorenz U. (2009). SHP-1 and SHP-2 in T cells: two phosphatases functioning at many levels. Immunol. Rev 228, 342–359. 10.1111/j.1600-065X.2008.00760.x. [PubMed: 19290938]
67. Goel S, DeCristo MJ, Watt AC, BrinJones H, Sceneay J, Li BB, Khan N, Ubellacker JM, Xie S, Metzger-Filho O, et al. (2017). CDK4/6 inhibition triggers anti-tumour immunity. Nature 548, 471–475. 10.1038/nature23465. [PubMed: 28813415]
68. Deng J, Wang ES, Jenkins RW, Li S, Dries R, Yates K, Chhabra S, Huang W, Liu H, Aref AR, et al. (2018). CDK4/6 inhibition augments antitumor immunity by enhancing T-cell activation. Cancer Discov. 8, 216–233. 10.1158/2159-8290.CD-17-0915. [PubMed: 29101163]
69. Heckler M, Ali LR, Clancy-Thompson E, Qiang L, Ventre KS, Lenehan P, Roehle K, Luoma A, Boelaars K, Peters V, et al. (2021). Inhibition of CDK4/6 promotes CD8 T-cell memory formation. Cancer Discov. 11, 2564–2581. 10.1158/2159-8290.CD-20-1540. [PubMed: 33941591]
70. Lelliott EJ, Kong IY, Zethoven M, Ramsbottom KM, Martelotto LG, Meyran D, Zhu JJ, Costacurta M, Kirby L, Sandow JJ, et al. (2021). CDK4/6 inhibition promotes antitumor immunity through the induction of T-cell memory. Cancer Discov. 11, 2582–2601. 10.1158/2159-8290.CD-20-1554. [PubMed: 33990344]
71. Liu R, Mathieu C, Berthelet J, Zhang W, Dupret JM, and Rodrigues Lima F. (2022). Human protein tyrosine phosphatase 1B (PTP1B): from structure to clinical inhibitor perspectives. Int. J. Mol. Sci 23, 7027. 10.3390/ijms23137027. [PubMed: 35806030]

72. Brandão TAS, Hengge AC, and Johnson SJ (2010). Insights into the reaction of protein-tyrosine phosphatase 1B: crystal structures for transition state analogs of both catalytic steps. J. Biol. Chem 285, 15874–15883. 10.1074/jbc.M109.066951. [PubMed: 20236928]
73. Tabernero L, Aricescu AR, Jones EY, and Szedlacsek SE (2008). Protein tyrosine phosphatases: structure-function relationships. FEBS J. 275, 867–882. 10.1111/j.1742-4658.2008.06251.x. [PubMed: 18298793]
74. Daniels MA, and Teixeiro E. (2015). TCR signaling in T cell memory. Front. Immunol 6, 617. 10.3389/fimmu.2015.00617. [PubMed: 26697013]
75. Kaech SM, Wherry EJ, and Ahmed R. (2002). Effector and memory T-cell differentiation: implications for vaccine development. Nat. Rev. Immunol 2, 251–262. 10.1038/nri778. [PubMed: 12001996]
76. Isakov N, and Altman A. (2002). Protein kinase C(theta) in T cell activation. Annu. Rev. Immunol 20, 761–794. 10.1146/annurev.immunol.20.100301.064807. [PubMed: 11861617]
77. Takahama Y, and Nakauchi H. (1996). Phorbol ester and calcium ionophore can replace TCR signals that induce positive selection of CD4 T cells. J. Immunol 157, 1508–1513. [PubMed: 8759732]
78. Penafuerte C, Feldhammer M, Mills JR, Vinette V, Pike KA, Hall A, Migon E, Karsenty G, Pelletier J, Zogopoulos G, and Tremblay ML (2017). Downregulation of PTP1B and TC-PTP phosphatases potentiate dendritic cell-based immunotherapy through IL-12/IFNgamma signaling. OncoImmunology 6, e1321185. 10.1080/2162402X.2017.1321185. [PubMed: 28680757]
79. Heinonen KM, Bourdeau A, Doody KM, and Tremblay ML (2009). Protein tyrosine phosphatases PTP-1B and TC-PTP play nonredundant roles in macrophage development and IFN-gamma signaling. Proc. Natl. Acad. Sci. USA 106, 9368–9372. 10.1073/pnas.0812109106. [PubMed: 19474293]
80. Wiede F, Lu KH, Du X, Zeissig MN, Xu R, Goh PK, Xirouchaki CE, Hogarth SJ, Greatorex S, Sek K, et al. (2022). PTP1B is an intracellular checkpoint that limits T-cell and CAR T-cell antitumor immunity. Cancer Discov. 12, 752–773. 10.1158/2159-8290.CD-21-0694. [PubMed: 34794959]
81. Wiede F, Lu KH, Du X, Liang S, Hochheiser K, Dodd GT, Goh PK, Kearney C, Meyran D, Beavis PA, et al. (2020). PTPN2 phosphatase deletion in T cells promotes anti-tumour immunity and CAR T-cell efficacy in solid tumours. EMBO J. 39, e103637. 10.15252/embj.2019103637. [PubMed: 31803974]
82. LaFleur MW, Nguyen TH, Coxe MA, Miller BC, Yates KB, Gillis JE, Sen DR, Gaudiano EF, Al Abosy R, Freeman GJ, et al. (2019). PTPN2 regulates the generation of exhausted CD8(+) T cell subpopulations and restrains tumor immunity. Nat. Immunol 20, 1335–1347. 10.1038/s41590-019-0480-4. [PubMed: 31527834]
83. McGuire K, Baumgartner C, Backus C, Mathew R, Klinge K, Klahn J, Geda P, Halliwill K, Aguado J, Mu L, et al. (2022). 1365 an active site PTPN2/N1 small molecule inhibitor promotes anti-tumor efficacy by sensitizing tumor cells to inflammatory signals and enhancing immune cell activity. Journal for ImmunoTherapy of Cancer 10, A1416. 10.1136/jitc-2022-SITC2022.1365.
84. Iracheta-Vellve A, Ebrahimi-Nik H, Davis TR, Olander KE, Kim SY, Yeary MD, Patti JC, Kohnle IC, Baumgartner CK, Hamel KM, et al. (2022). Abstract 606: targeting the immune checkpoint PTPN2 with ABBV-CLS-484 inflames the tumor microenvironment and unleashes potent CD8+ T cell immunity. Cancer Res. 82, 606. 10.1158/1538-7445.Am2022-606.
85. Baumgartner CK, Paddock MN, Frost JM, Hamel KM, McGuire KA, Halliwill K, Xiong Z, Mu L, Klinge K, Geda P, et al. (2022). Abstract ND06: ABBV-CLS-484: an active site PTPN2/N1 inhibitor that augments the immune response and sensitizes tumors to immune-mediated killing. Cancer Res. 82, ND06. 10.1158/1538-7445.Am2022-nd06.
86. Tsutsui T, Hesabi B, Moons DS, Pandolfi PP, Hansel KS, Koff A, and Kiyokawa H. (1999). Targeted disruption of CDK4 delays cell cycle entry with enhanced p27(Kip1) activity. Mol. Cell Biol 19, 7011–7019. 10.1128/MCB.19.10.7011. [PubMed: 10490638]
87. Sicinski P, Donaher JL, Parker SB, Li T, Fazeli A, Gardner H, Haslam SZ, Bronson RT, Elledge SJ, and Weinberg RA (1995). Cyclin D1 provides a link between development and oncogenesis in the retina and breast. Cell 82, 621–630. 10.1016/0092-8674(95)90034-9. [PubMed: 7664341]

88. Sicinski P, Donaher JL, Geng Y, Parker SB, Gardner H, Park MY, Robker RL, Richards JS, McGinnis LK, Biggers JD, et al. (1996). Cyclin D2 is an FSH-responsive gene involved in gonadal cell proliferation and oncogenesis. Nature 384, 470–474. 10.1038/384470a0. [PubMed: 8945475]

89. Sicinska E, Aifantis I, Le Cam L, Swat W, Borowski C, Yu Q, Ferrando AA, Levin SD, Geng Y, von Boehmer H, and Sicinski P. (2003). Requirement for cyclin D3 in lymphocyte development and T cell leukemias. Cancer Cell 4, 451–461. 10.1016/s1535-6108(03)00301-5. [PubMed: 14706337]

90. Li T, Fan J, Wang B, Traugh N, Chen Q, Liu JS, Li B, and Liu XS (2017). TIMER: a web server for comprehensive analysis of tumor-infiltrating immune cells. Cancer Res. 77, e108–e110. 10.1158/0008-5472.CAN-17-0307. [PubMed: 29092952]

91. Seo N, Tokura Y, Nishijima T, Hashizume H, Furukawa F, and Takigawa M. (2000). Percutaneous peptide immunization via corneum barrier-disrupted murine skin for experimental tumor immunoprophylaxis. Proc. Natl. Acad. Sci. USA 97, 371–376. 10.1073/pnas.97.1.371. [PubMed: 10618425]

92. van Stipdonk MJB, Badia-Martinez D, Sluijter M, Offringa R, van Hall T, and Achour A. (2009). Design of agonistic altered peptides for the robust induction of CTL directed towards H-2Db in complex with the melanoma-associated epitope gp100. Cancer Res. 69, 7784–7792. 10.1158/0008-5472.CAN-09-1724. [PubMed: 19789338]

93. Ly LV, Sluijter M, van der Burg SH, Jager MJ, and van Hall T. (2013). Effective cooperation of monoclonal antibody and peptide vaccine for the treatment of mouse melanoma. J. Immunol 190, 489–496. 10.4049/jimmunol.1200135. [PubMed: 23203930]

94. Kim MV, Ouyang W, Liao W, Zhang MQ, and Li MO (2014). Murine in vitro memory T cell differentiation. Bio. Protoc 4, e1171. 10.21769/BioProtoc.1171.

95. Moore T, Wagner CR, Scurti GM, Hutchens KA, Godellas C, Clark AL, Kolawole EM, Hellman LM, Singh NK, Huyke FA, et al. (2018). Clinical and immunologic evaluation of three metastatic melanoma patients treated with autologous melanoma-reactive TCR-transduced T cells. Cancer Immunol. Immunother 67, 311–325. 10.1007/s00262-017-2073-0. [PubMed: 29052782]

96. Norell H, Zhang Y, McCracken J, Martins da Palma T, Lesher A, Liu Y, Roszkowski JJ, Temple A, Callender GG, Clay T, et al. (2010). CD34-based enrichment of genetically engineered human T cells for clinical use results in dramatically enhanced tumor targeting. Cancer Immunol. Immunother 59, 851–862. 10.1007/s00262-009-0810-8. [PubMed: 20052466]

97. McAlister GC, Nusinow DP, Jedrychowski MP, Wühr M, Huttlin EL, Erickson BK, Rad R, Haas W, and Gygi SP (2014). MultiNotch MS3 enables accurate, sensitive, and multiplexed detection of differential expression across cancer cell line proteomes. Anal. Chem 86, 7150–7158. 10.1021/ac502040v. [PubMed: 24927332]

98. Huttlin EL, Jedrychowski MP, Elias JE, Goswami T, Rad R, Beausoleil SA, Villén J, Haas W, Sowa ME, and Gygi SP (2010). A tissue-specific atlas of mouse protein phosphorylation and expression. Cell 143, 1174–1189. 10.1016/j.cell.2010.12.001. [PubMed: 21183079]

99. Eng JK, McCormack AL, and Yates JR (1994). An approach to correlate tandem mass spectral data of peptides with amino acid sequences in a protein database. J. Am. Soc. Mass Spectrom 5, 976–989. 10.1016/1044-0305(94)80016-2. [PubMed: 24226387]

100. Elias JE, and Gygi SP (2007). Target-decoy search strategy for increased confidence in large-scale protein identifications by mass spectrometry. Nat. Methods 4, 207–214. 10.1038/nmeth1019. [PubMed: 17327847]

101. Ting L, Rad R, Gygi SP, and Haas W. (2011). MS3 eliminates ratio distortion in isobaric multiplexed quantitative proteomics. Nat. Methods 8, 937–940. 10.1038/nmeth.1714. [PubMed: 21963607]

102. Fu J, Li K, Zhang W, Wan C, Zhang J, Jiang P, and Liu XS (2020). Large-scale public data reuse to model immunotherapy response and resistance. Genome Med. 12, 21. 10.1186/s13073-020-0721-z. [PubMed: 32102694]

Highlights

- CDK6 expression in the tumor microenvironment shapes a pro-tumor microenvironment
- CDK6 activates PTP1B and TCPTP to de-phosphorylate CD3ζ and decrease T cell activity
- Targeting PTPs lessens resistance to immunotherapy
- Targeting PTPs may augment adoptive T cell therapy for cancer patients

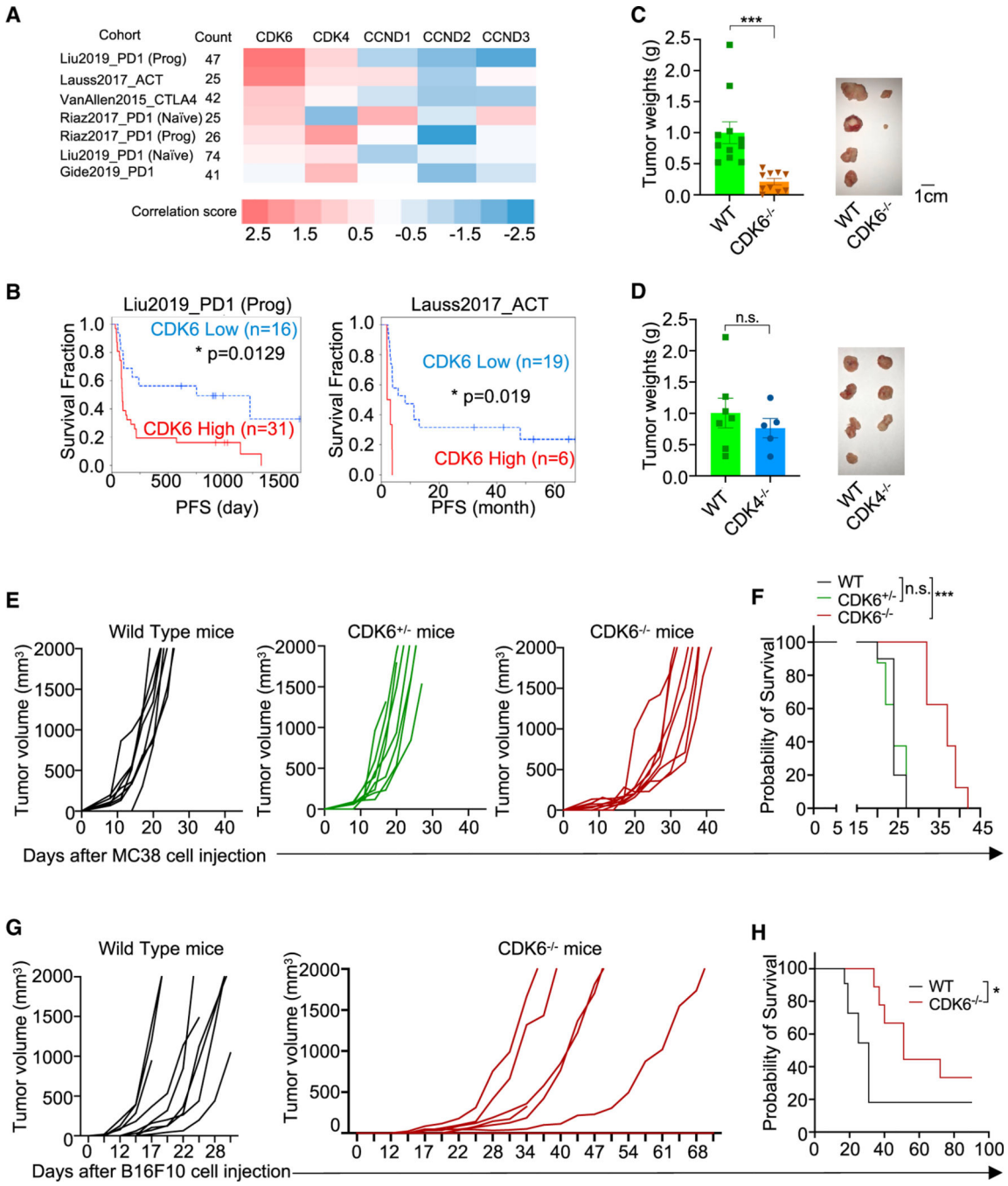

Figure 1. High CDK6 expression correlates with immunotherapy resistance, and CDK6 ablation in the TME inhibits tumor growth

(A) CDK6 expression was positively correlated with risk of death in 6 of 7 immunotherapy studies for melanoma patients analyzed with the Tumor Immune Dysfunction and Exclusion (TIDE) software.

(B) Two clinical studies showed that high CDK6 expression is significantly associated with poor PFS in patients treated with anti-PD1 Abs or ACT.

(C and D) Graphs of MC38 tumor weights from CDK6 (C, left) or CDK4 (D, left) KO mice. Tumors were harvested on day 15. Also shown are representative tumors from WT and KO

mice (C and D, right). CDK6 KO, n = 10; CDK6 WT, n = 11; CDK4 KO, n = 7; CDK4 WT, n = 5.

(E and F) CDK6 ablation in the TME inhibited MC38 tumor growth. Shown are tumor growth curves from individual mice (E) and survival (F) of tumor-bearing mice. n = 8 mice/group.

(G and H) CDK6 ablation in the TME inhibited B16F10 melanoma tumor growth. Shown are tumor growth curves (G) and overall survival of tumor-bearing mice (H). CDK6 KO, n = 9; WT, n = 11.

(C) and (D) show mean ± SEM, two-tailed Student's t test. Each dot represents an individual mouse. *$p < 0.05$, ***$p < 0.001$; n.s., not significant.

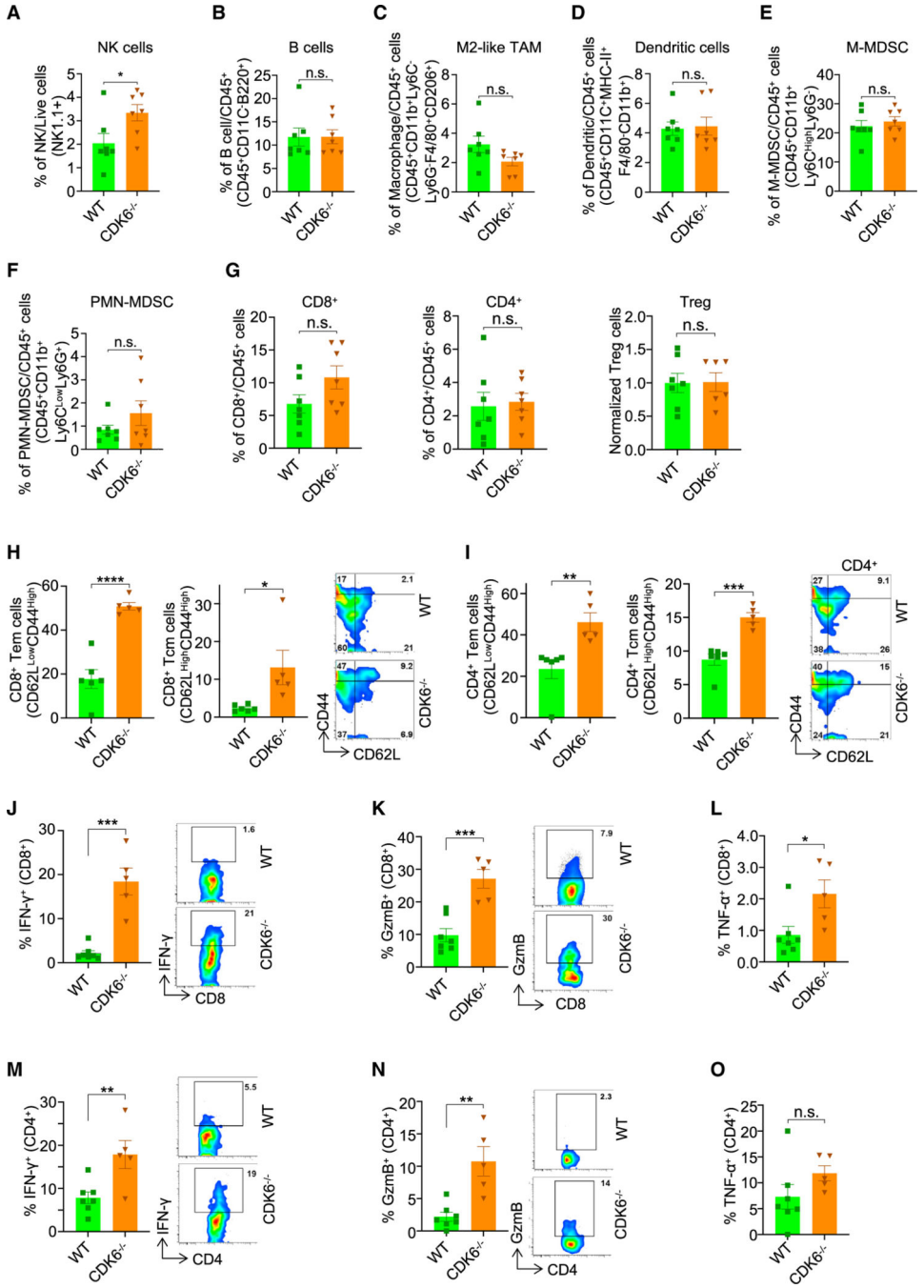

Figure 2. CDK6 depletion in the TME reshapes the tumor immune microenvironment and increases tumor-infiltrating T cell cytotoxicity

(A–F) Comparison of cell populations of the TME in MC38 tumors derived from CDK6 KO or WT littermate controls. n = 7.

(G) Relative amounts of tumor-infiltrating $CD8^+$, $CD4^+$, and Treg cells from CDK6 KO or WT littermate controls. Treg, $CDK6^{-/-}$, n = 6; others, n = 7.

(H and I) Comparative analysis of memory T cells among $CD8^+$ (H) or $CD4^+$ (I) tumor-infiltrating T cells from CDK6 KO or WT littermate controls. Shown are representative flow cytometry plots (right). CDK6 KO, n = 5; WT, n = 6.

(J–O) Activities of $CD8^+$ (J–L) or $CD4^+$ (M–O) tumor-infiltrating T cells isolated from CDK6 KO or WT mice. IFN-γ (J and M), GzmB (K and N), and TNF-α (L and O) were detected with flow cytometry. CDK6 KO, n = 5; WT, n = 7.

Mean ± SEM, two-tailed Student's t test. *p < 0.05, **p < 0.01, ***p < 0.001, ****p < 0.0001.

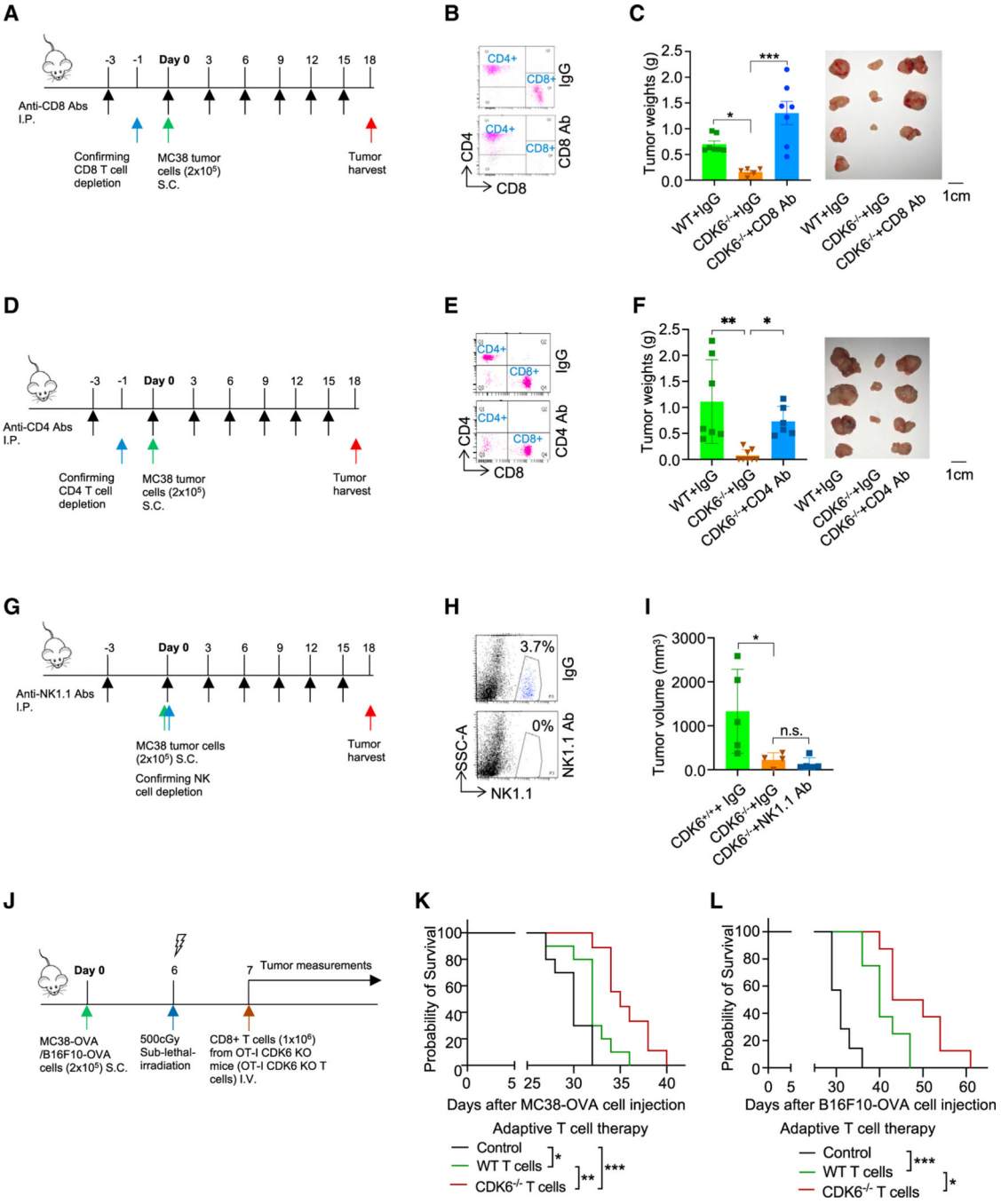

Figure 3. Depletion of CD8$^+$ or CD4$^+$ T cells reverses the host antitumor effects in CDK6 KO mice

(A and D) Schematic timeline for pre-depletion of CD8$^+$ (A) or CD4$^+$ (D) T cells with anti-CD8 (A) or anti-CD4 (D) Abs in CDK6 KO mice.

(B and E) Representative flow cytometry assays showing pre-depletion of CD8$^+$ (B) or CD4$^+$ (E) T cells.

(C and F) Pre-depletion of CD8$^+$ (C) or CD4$^+$ (F) T cells reversed the host anti-tumor effect in CDK6 KO mice. Shown are MC38 tumor weights (left) and representative tumors (right). n ≥ 5 (C), n ≥ 6 (F).

(G) Schematic timeline for NK cell depletion with anti-NK1.1 Abs in CDK6 KO mice.
(H and I) Pre-depletion of NK cells did not affect the host anti-tumor effect in CDK6 KO mice. Representative flow cytometry assays show pre-depletion of NK cells (H). MC38 tumor volumes from mice are also shown (I). $n \geq 4$.
(J) Schematic timeline for adoptive T cell therapy.
(K and L) Survival of mice challenged with MC38-OVA (K) or B16F10-OVA (L) receiving an adoptive transfer of CDK6 KO (red lines) or WT (green lines) OT-I $CD8^+$ T cells. Tumor-bearing mice that received no therapy served as controls (black lines). $n \geq 9$ (K), $n \geq 7$ (L).
(C), (F), and (I) represent mean ± SEM; 1-way ANOVA (Dunnett test). *$p < 0.05$, **$p < 0.01$, ***$p < 0.001$.

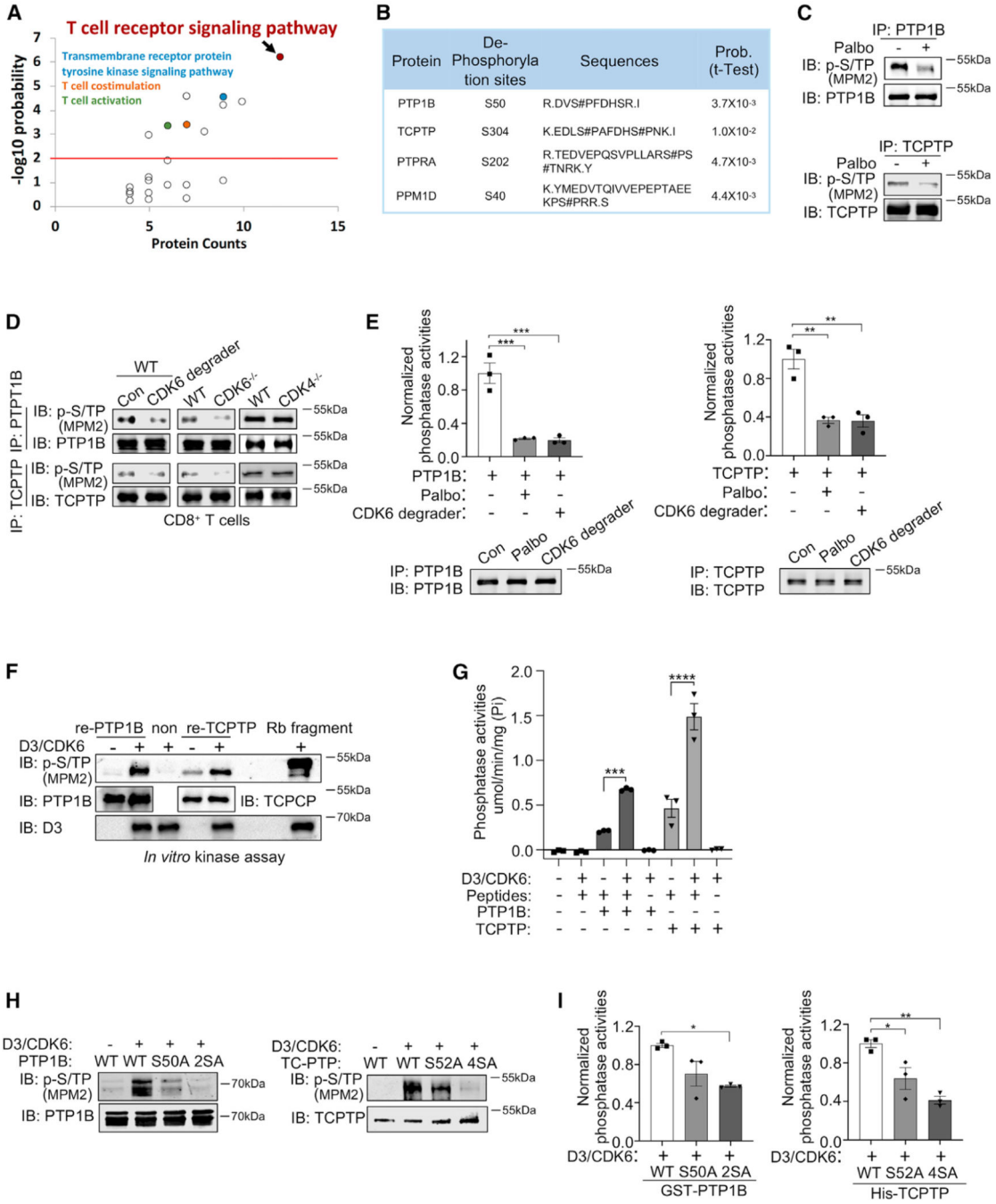

Figure 4. CDK6 inhibition increases tyrosine phosphorylation of proteins functioning in TCR signaling, and cyclin D3/CDK6 phosphorylates/activates PTP1B and TCPTP

(A) GO enrichment analysis of TMT-MS data showed the top-ranked annotation groups among increased tyrosine-phosphorylated proteins in KOPTK1 cells upon treatment with palbociclib. 13 of 105 tyrosine-phosphorylated proteins relate to the TCR signaling pathway.

(B) A list of PTPs, derived from TMT-MS data analysis, dephosphorylated at S/TP phosphorylation sites.

(C) IB with anti-phospho-S/TP Abs of PTP1B or TCPTP immunoprecipitated from KOPTK1 cells treated with palbociclib (24 h).

(D) IB with anti-phospho-S/TP Abs of immunoprecipitated PTP1B or TCPTP from interleukin-2 (IL-2)/CD3-activated splenic $CD8^+$ T cells isolated from WT, CDK6 KO (center), or CDK4 KO mice (right) or from WT $CD8^+$ T cells treated with vehicle or a CDK6 degrader (BSJ-03–123, 10 μM) for 24 h (left).
(E) Phosphatase activities of PTP1B (left) and TCPTP (right) immunoprecipitated from Jurkat cells treated with a CDK4/6 inhibitor (palbociclib,1 μM) or CDK6 degrader (BSJ-03–123, 10 μM) for 24 h. Immunoblotting of PTP1B or TCPTP following immunoprecipitation (IP) shows protein loading of PTPs.
(F) IB of recombinant PTP1B or TCPTP protein phosphorylated by cyclin D3/CDK6 following an *in vitro* kinase assay with anti-phospho-S/TP Abs. The recombinant Rb fragment was a positive control.
(G) Phosphatase activities of PTP1B and TCPTP with or without cyclin D3/CDK6 phosphorylation.
(H) IB with anti-phospho-S/TP Abs following kinase assays showed that PTP mutants were not or less phosphorylated by cyclin D3/CDK6 compared with the corresponding WT PTP.
(I) Normalized phosphatase activities of PTP mutants following kinase assays with cyclin D3/CDK6.
(E), (G), and (I) represent mean ± SEM; 1-way ANOVA (Dunnett's test) (E and G) and two-tailed Student's t test (I). n = 3 (E, G, and I). *$p < 0.05$, **$p < 0.01$, ***$p < 0.001$, ****$p < 0.0001$.

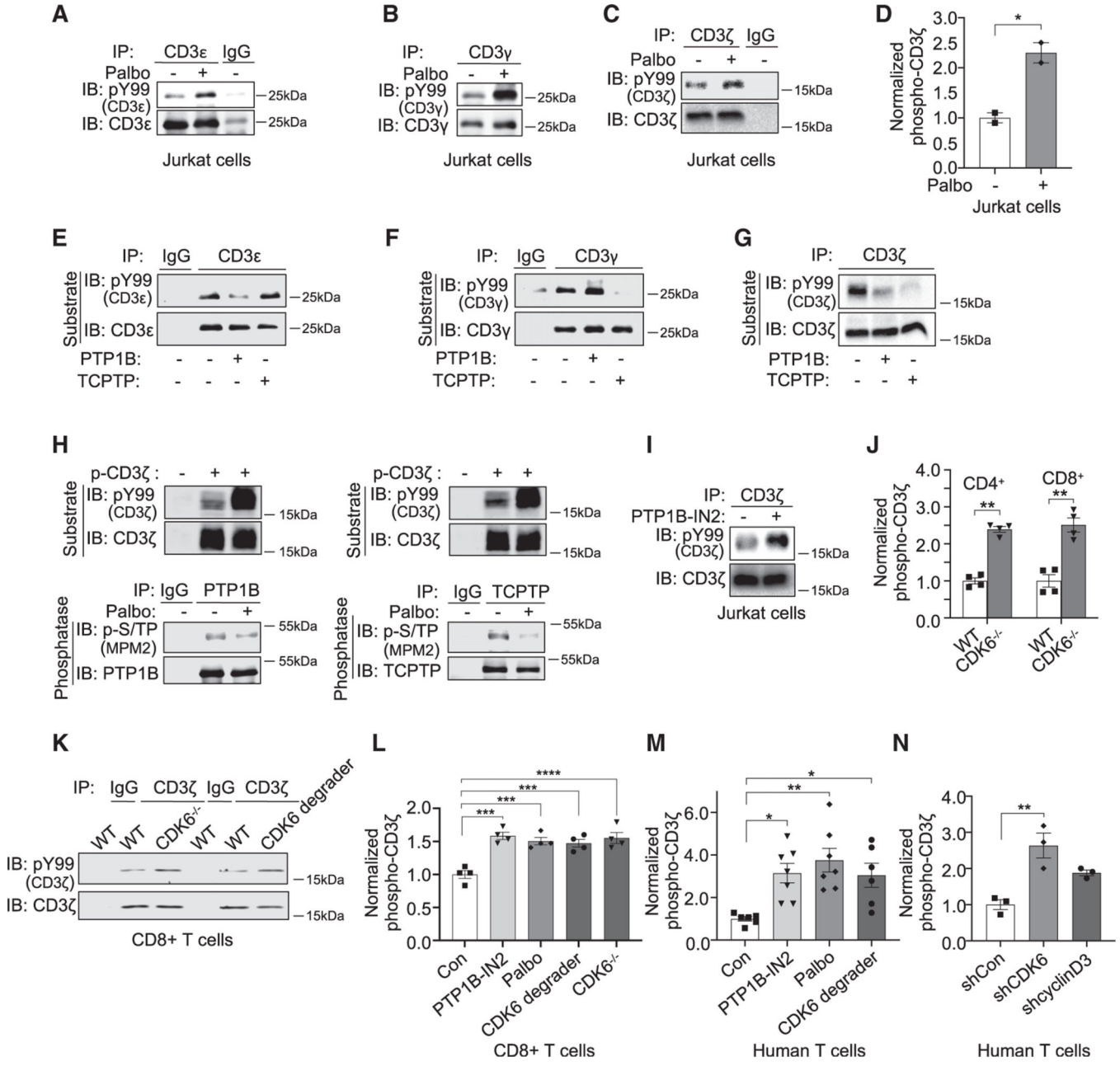

Figure 5. CDK6 inhibition increases CD3ζ tyrosine phosphorylation mediated by PTP1B and TCPTP

(A–C) Immunoprecipitation using Abs specific to CD3ε, CD3γ, or CD3ζ, followed by immunoblotting using pY99 phosphotyrosine Abs to detect phosphorylation of CD3 subunits in Jurkat cells treated with palbociclib (24 h).

(D) Comparative CD3ζ phosphorylation measured with flow cytometry by phospho-Tyr142 Abs in Jurkat cells with and without palbociclib treatment (24 h). n = 2.

(E–G) *In vitro* phosphatase assay showed that CD3ε, CD3γ, and CD3ζ were the substrates of PTP1B and/or TCPTP.

(H) *In vitro* phosphatase assay to detect the phosphatase activity of PTP1B or TCPTP immunoprecipitated from Jurkat cells treated with palbociclib (8 h). The phosphorylation level of PTP1B/TCPTP was detected using p-S/TP Abs.

(I) IB using pY99 to detect phosphorylated CD3ζ immunoprecipitated from Jurkat cells treated with PTP1B-IN2 (1 μM, 24 h).

(J) Phosphorylation levels of CD3ζ at Tyr142 in CD3/CD28/IL-2-activated splenic $CD4^+$ or $CD8^+$ T cells from CDK6 KO mice or WT littermates. n = 4.

(K) IB of tyrosine phosphorylation of CD3ζ in $CD8^+$ T cells from CDK6 KO mice or WT littermates or in WT $CD8^+$ T cells treated with a CDK6 degrader for 48 h (L and M) Comparative levels of tyrosine phosphorylated CD3ζ (phospho-CD3ζ [Tyr142] Abs) in OVA peptide-activated $CD8^+$ T cells isolated from OT-I mice (L) or primary human T cells derived from peripheral blood mononuclear cells (M) upon treatment with PTP1B-IN2 (1 μM), palbociclib (1 μM), or BSJ-03–123 (5 μM) for 24 h n = 4 (L). Con, n = 6; PTPIB-IN2, n = 7; palbociclib (Palbo), n = 7; CDK6 degrader, n = 6 (M).

(N) Phosphorylation levels of CD3ζ at Tyr142 in human T cells upon genetic deletion of CDK6 (shCDK6) or cyclin D3 (shcyclinD3). n = 3.

(D), (J), and (L)–(N) represent mean ± SEM; two-tailed Student's t-test (D and J) and 1-way ANOVA (Dunnett's test) (L–N); *p < 0.05, **p < 0.01, ***p < 0.001, ****p < 0.0001.

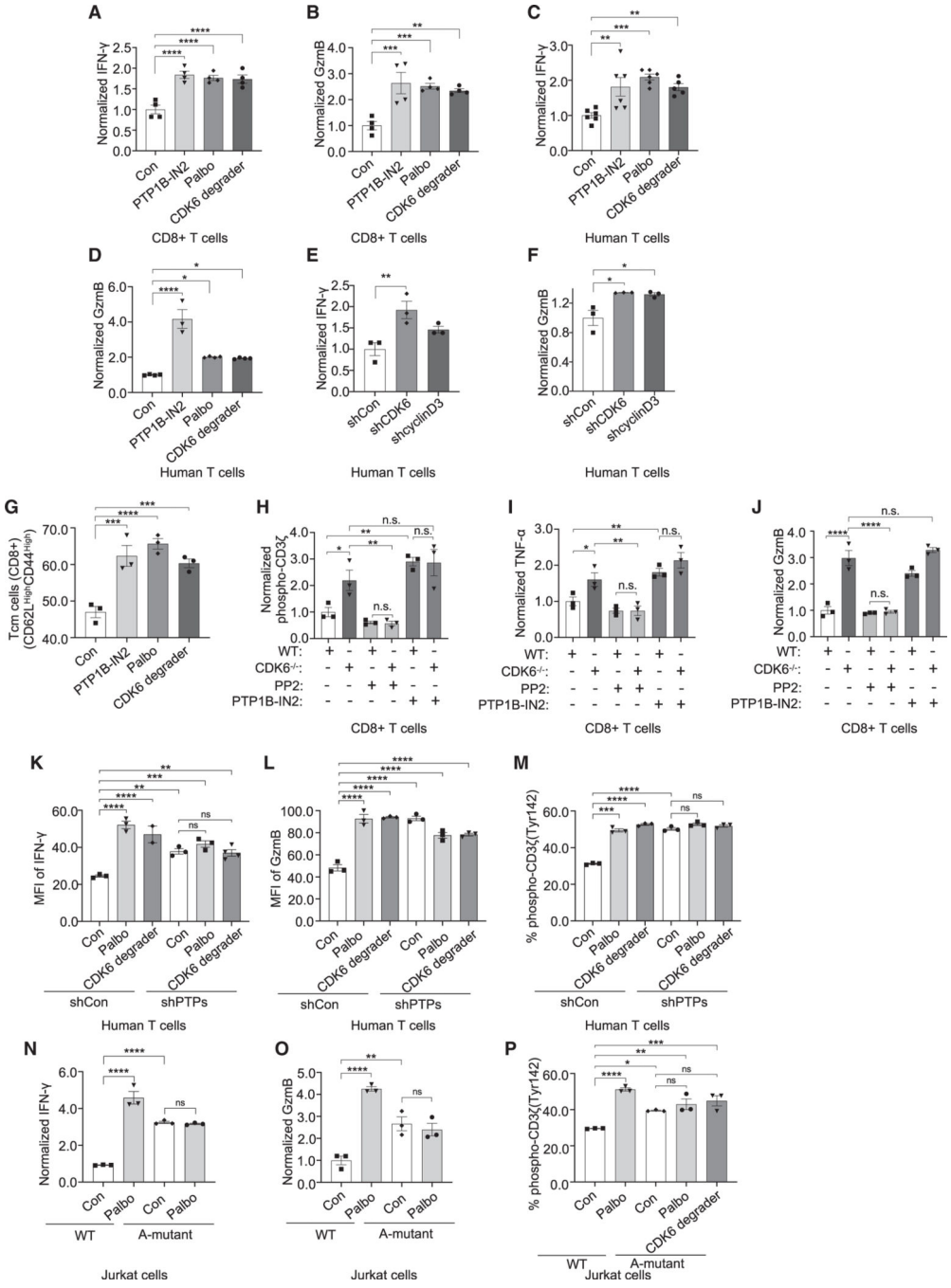

Figure 6. Cyclin D3/CDK6 depletion or PTP1B/TCPTP inhibition increases cytokine production in T cells

(A–D) Bar graphs show a comparison of IFN-γ (A and C) and GzmB (B and D) production of T cells treated with 1 μM PTPIB-IN2, 1 μM Palbo, or 10 μM BSJ-03–123 for 24 h. In (D), 2 μM PTPIB-IN2 was applied for 16 h. $CD8^+$ T cells were isolated from OT-I mice (A and B) or human T cells (C and D). n = 4 (A), n = 4 (B), n ≥ 5 (C), n ≥ 3 (D).

(E and F) Normalized IFN-γ (E) or GzmB (F) production in human T cells in which cyclin D3 or CDK6 was knocked down.

(G) The population of memory T cells differentiated from T cells upon treatment with PTP1B-IN2 (0.5 μM), Palbo (0.5 μM), or BSJ-03–123 (5 μM) for 2 days in the presence of IL-15.

(H–J) Bar graphs show a comparison of phospho-Tyr142 of CD3ζ (H), TNF-α (I), and GzmB (J) of T cells treated with inhibitors for LCK kinase (10 μM PP2) or PTPs (1 μM PTPIB-IN2) for 4 h

(K–P) Bar graphs show a comparison of IFN-γ (K and N) and GzmB (L and O) production and phospho-Tyr142 of CD3ζ levels (M and P) of PTP knockdown (K–M) or A-mutant expressing (N–P) T cells treated with 1 μM Palbo or 5 μM BSJ-03–123 for 24 h

$n \geq 2$ (E–P). Mean ± SEM, 1-way ANOVA (Dunnett's test). *$p < 0.05$, **$p < 0.01$, ***$p < 0.001$, ****$p < 0.0001$.

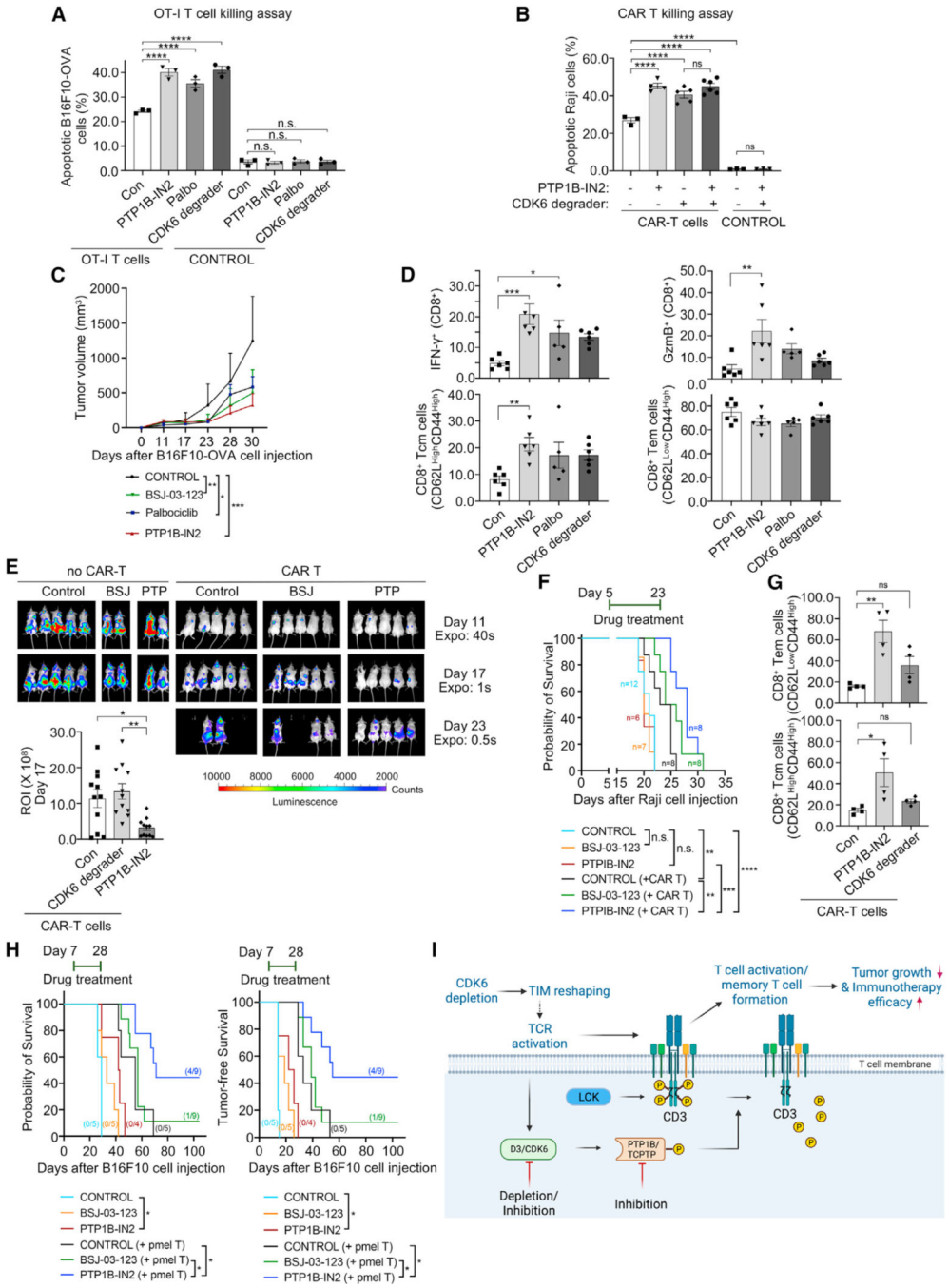

Figure 7. Targeting the CDK6-PTPs axis enhances the efficacy of T cell killing and adoptive T cell immunotherapy

.

(A) *In vitro* tumor killing assays showed that targeting the CDK6-PTPs axis increased splenic $CD8^+$ T cell killing capacity against OVA-expressing B16F10 cells. The control groups were without OT-I $CD8^+$ T cells. n = 3.

(B) CAR T tumor killing assay was applied to examine the cytotoxicity of human T cells targeting Raji cells expressing GFP upon compound treatments. n ≥ 3. For (A) and (B), 1 μM PTP1B-IN2, 1 μM Palbo, or 10 μM BSJ-03–123 was applied.

(C) Graph showing the mean of B16F10-OVA tumor volumes in C57BL/6-Ly5.1 mice receiving $CD8^+$ T cells from OT-I mice. $n \geq 5$.

(D) Activities of tumor-infiltrating OT-I $CD8^+$ T cells (top) and analysis of memory T cells among tumor-infiltrating OT-I T cells from C57BL/6-Ly5.1 mice (bottom). $Ly5.2^+$ T cells were quantified in this experiment. $n \geq 5$.

(E and F) Bioluminescence images (E) and overall survival graph (F) of tumor progression in Raji tumor-bearing mice with/without receiving CAR T cells under treatment with BSJ-03–123 (50 mg/kg) or PTP1B-IN2 (5 mg/kg). Shown are representative bioluminescence images (E, top) and quantification of the regions of interest (ROIs) (E, bottom). n = 11/group.

(G) Memory T cell analysis of CAR T cells from Raji tumor-bearing mice receiving treatment with PTP1B-IN2 or BSJ-03–123 for 2 weeks. n = 4/group.

(H) Overall survival (left) and tumor-free survival (right) of mice challenged with B16F10 melanoma cells with/without receiving pmel $CD8^+$ T cells.

(I) Schematic depicting the presented study model. Created with BioRender.

(A), (B), (D), and (G) represent mean ± SEM, 1-way ANOVA (Dunnett's test); *$p < 0.05$, **$p < 0.01$, ***$p < 0.001$, ****$p < 0.0001$.

KEY RESOURCES TABLE

REAGENT or RESOURCE	SOURCE	IDENTIFIER
Antibodies		
CDK6 Ab	Cell signaling	Cat# 3136; RRID:AB_2229289
CDK4 Ab	Thermo Fisher	Cat# MS-616-P1; RRID:AB_142551
Cyclin D1 Ab	Thermo Fisher	Cat# RB-010-P1; RRID:AB_60654
Cyclin D2 Ab	MBL International	Cat# K0064–3; RRID:AB_591184
cyclin D3 Ab	Abcam	Cat# ab28283; RRID:AB_2070798
PTP1B Ab	Proteintech	Cat# 11334–1-AP; RRID:AB_10642566
PTP1B Ab	Thermo Fisher	Cat# MA5–25642; RRID:AB_2725150
TCPTP Ab	Proteintech	Cat# 11214–1-AP; RRID:AB_2173235
TCPTP Ab	R&D	Cat# MAB1930; RRID:AB_2173232
p-MPM2 Ab	Millipore	Cat# 05–368; RRID:AB_309698
pY99 Ab	Santa Cruz Biotechnology	Cat# sc-7020; RRID:AB_628123
CD3ζ Ab	Proteintech	Cat# 12837–2-AP; RRID:AB_2244279
PPMID Ab	Santa Cruz Biotechnology	Cat# sc-376257; RRID:AB_10986000
PTPRA Ab	Santa Cruz	Cat# sc-398203
tubulin Ab	Sigma-Aldrich	Cat# T9026; RRID:AB_477593
GST Ab	Cell Signaling Technology	Cat# 2622; RRID:AB_331670
GAPDH Ab	Cell Signaling Technology	Cat# 5174; RRID:AB_10622025
HIS Ab	Santa Cruz Biotechnology	Cat# SC-803; RRID:AB_631655
p-RB Ab	Cell Signaling Technology	Cat# 9307; RRID:AB_330015
SHP-1 Ab	Thermo Fisher Scientific	Cat# MA1–21484; RRID:AB_2173724
SHP-1 Ab	Proteintech	Cat# 24546–1-AP; RRID:AB_2879600
SHP-2 Ab	Thermo Fisher Scientific	Cat# MA5–17160; RRID:AB_2538631
SHP-2 Ab	Proteintech	Cat# 20145–1-AP; RRID:AB_10699877
APC/Cyanine7 anti-mouse CD4 Ab	BioLegend	Cat# 100526; RRID:AB_312727
Alexa Fluor(R) 700 anti-mouse CD8a Ab	BioLegend	Cat# 100730; RRID:AB_493703
CD44 Ab	BD Biosciences	Cat# 563971; RRID:AB_2738518
PE anti-mouse CD62L Ab	BioLegend	Cat# 104407; RRID:AB_313094
PerCP/Cyanine5.5 anti-mouse TCR beta chain Ab	BioLegend	Cat# 109228; RRID:AB_1575173
PerCP/Cyanine5.5 anti-mouse CD45 Ab	BioLegend	Cat# 103131; RRID:AB_893344
MHC-II Ab	BD Biosciences	Cat# 562011; RRID:AB_10894585
CD11b Ab	BD Biosciences	Cat# 561098; RRID:AB_2033994
APC/Cyanine7 anti-mouse CD11c Ab	BioLegend	Cat# 117323; RRID:AB_830646
BV711 anti-mouse F4/80 Ab	BD Biosciences	Cat# 565612; RRID:AB_2734769
Brilliant Violet 421(TM) anti-mouse/human CD45R/B220 Ab	BioLegend	Cat# 103251; RRID:AB_2562905
Rat anti-mouse Ly-6C Ab, APC Conjugated, Clone AL-21	BD Biosciences	Cat# 560595; RRID:AB_1727554
PE anti-mouse CD206 (MMR) Ab	BioLegend	Cat# 141705; RRID:AB_10896421
Alexa Fluor(R) 700 anti-mouse Ly-6G Ab	BioLegend	Cat# 127621; RRID:AB_10640452
Brilliant Violet 711(TM) anti-mouse NK-1.1 Ab	BioLegend	Cat# 108745; RRID:AB_2563286

REAGENT or RESOURCE	SOURCE	IDENTIFIER
Rat anti-TNF Ab, Allophycocyanin Conjugated, Clone MP6-XT22	BD Biosciences	Cat# 554420; RRID:AB_398553
Phospho-CD247 (CD3 zeta) (Tyr142) Ab (3ZBR4S), PE, eBioscience	Thermo Fisher Scientific	Cat# 12–2478-42; RRID:AB_2744700
FITC anti-mouse IFN-gamma Ab	BioLegend	Cat# 505806; RRID:AB_315400
PE anti-mouse IL-2 Ab	BioLegend	Cat# 503808; RRID:AB_315302
FITC anti-human/mouse Granzyme B Ab	BioLegend	Cat# 515403; RRID:AB_2114575
Ki67 Ab	BD Biosciences	Cat# 561281; RRID:AB_10613816
PE anti-mouse FOXP3 Ab	BioLegend	Cat# 126404; RRID:AB_1089117
CD8 Ab	Bio X Cell	Cat# BE0061; RRID:AB_1125541
CD4 Ab	Bio X Cell	Cat# BE0003–1; RRID:AB_1107636
IgG control	Bio X Cell	Cat# BE0090; RRID:AB_1107780
PerCP/Cyanine5.5 anti-human CD4 Ab	BioLegend	Cat# 317428; RRID:AB_1186122
APC/Cyanine7 anti-human CD8 Ab	BioLegend	Cat# 344714; RRID:AB_2044006
PE anti-human CD34 Ab	BioLegend	Cat# 343606; RRID:AB_1732008
Anti-human CD45RA antibody, V450 Conjugated	BD Biosciences	Cat# 560363; RRID:AB_1645576
PE/Cyanine7 anti-human CD45RO Ab	BioLegend	Cat# 304230; RRID:AB_11203900
APC anti-human CD197 (CCR7) Ab	BioLegend	Cat# 353214; RRID:AB_10917387
BrdU Ab	BD Biosciences	Cat# 556028; RRID:AB_396304
Chemicals, peptides, and recombinant proteins		
BSJ-03–123	MedChemExpress	HY-111556
Palbociclib	MedChemExpress	HY-50767A
PTP1B-IN2	MedChemExpress	HY-100462
PP2	MedChemExpress	HY-13805
LIVE/DEAD yellow staining kit	Invitrogen	L34965
CD16/32 blocking FC	VWR	101302
Leukocyte Activation Cocktail	Fisher	BDB550583
Foxp3 fixation/permeabilization buffer	Fisher	00552300
CD3ε	BD	553057
CD28	BD	553294
Human interleukin-2	NCI	N/A
Cyclin D3/CDK6 protein kinase	Millipore	14–519
Cyclin D2/CDK4 protein kinase	ProQinase	0142–0375-1
Cyclin D2/CDK6 protein kinase	ProQinase	0051–0375-1
Cyclin D3/CDK4 protein kinase	ProQinase	0142–0373-1
PTP1B	VWR/R&D	1366-PT-050
TCPTP	VWR/R&D	1930-PT-050
OVA (257–264) peptide	AnaSpec	AS-60193–1
TRP-2 peptide	AnaSpec	AS-64811
Mouse IL-2	Miltenyi Biotec	130–120-333
(2-Hydroxypropyl)-β-cyclodextrin	Sigma	H5784
PEG300	Medchemexpress	HY-100462
Tween-80	Medchemexpress	HY-Y1891

REAGENT or RESOURCE	SOURCE	IDENTIFIER
IP lysis buffer	Pierce	87788
Protein protease inhibitors	Roche	11836170001
Phosphatase inhibitors	Roche	04906837001
Protein A/G PLUS-Agarose beads	Santa Cruz	sc-2003
RIPA buffer	Sigma	R0278
Protein assay dye	Bio-Rad	5000006
Collagenase Type IV	Gibco	17104–019
Red blood cell lysis buffer	BD	555899
Fixation buffer	BioLegend	420801
Ficoll-Paque PREMIUM (1.084 g/mL)	Fisher	45–001-755
EasySep buffer	Stemcell	20144
2-mercaptoethanol	Sigma	M7522
IL15	VWR (Biolegend)	566302
5-Bromo-2′-deoxyuridine (BrdU)	Sigma	B9285
propidium iodide (PI)	eBioscience	00–6990-50
Isopropyl-β-D-thiogalactoside (IPTG)	Sigma	I5502
Rb C-terminal protein	Santa Cruz	sc-4112
Tyrosine phosphatase substrate I	R&D	ES006
Fixation buffer	BioLegend	420801
gp100 (25–33) peptide	anaSpec	AS-62589
Critical commercial assays		
Leukocyte Reduction System (LRS) cones	Stemcell	200–0093
EasySep human T cell isolation kit	Stemcell	17951
ImmunoCult-XF T cell expansion medium	Stemcell	10981
human CD3/CD28 T cell activator	Stemcell	10971
Malachite green phosphate detection kit	R&D	DY996
Experimental models: Cell lines		
MC38	Zhang et al.[29]	N/A
B16F10	Zhang et al.[29]	N/A
Jurkat T	ATCC	TIB-152
KOPTK1	Wang et al.[30]	N/A
Raji	ATCC	CCL-86
Experimental models: Organisms/strains		
CDK6 constitutive knockout mice	Malumbres et al.[6]	N/A
CDK4 constitutive knockout mice	Tsutsui et al.[86]	N/A
Cyclin D1, constitutive knockout mice	Sicinski et al.[87]	N/A
Cyclin D2, constitutive knockout mice	Sicinski et al.[88]	N/A
Cyclin D3 constitutive knockout mice	Sicinska et al.[89]	N/A

REAGENT or RESOURCE	SOURCE	IDENTIFIER
Pmel mice	the Jackson Laboratory	Strain #:005023
C57BL/6 mice	the Jackson Laboratory	Strain #: 000664
C57BL/6-Ly5.1 mice	Charles river	Strain #: 564
OT-I transgenic mice	the Jackson Laboratory	Strain #: 003831
NSG mice	the Jackson Laboratory	Strain #: 005557
Oligonucleotides		
PTP1B-A181D: 5′-ctataccacatggcctg actttggagtccctgaat-3′	This manuscript	N/A
PTP1B-S50A: 5′-aaataggtacagagacg tcgctccctttgaccatagtcgg-3′	This manuscript	N/A
PTP1B-S205A: 5′-gtcagggtcactcgc cccggagcacggg-3′	This manuscript	N/A
TCPTP-S52A: 5′-gaaatcgaaacagatacag agatgtagccccatatgatcacagtc-3′	This manuscript	N/A
TCPTP-T261A: 5′-gaatgggtcttattcaggc cccagatcaactgaga-3′	This manuscript	N/A
TCPTP-S298A: 5′-ggaaagaactttctaaggaaga cttagctcctgcctttgatca-3′	This manuscript	N/A
TCPTP-S304A: 5′-gacttatctcctgcctttgatcatgc accaaacaaaataatgac-3′	This manuscript	N/A
Recombinant DNA		
shCDK4	Wang et al.[30]	N/A
shCDK6	Wang et al.[30]	N/A
shcyclin D3	Wang et al.[30]	N/A
shPTP1B	Sigma	TRCN0000320522
shTCPTP	Sigma	TRCN0000314612
PresentER-SIINFEKL (GFP)	Addgene	RRID:Addgene_102944
pPTP1BD181A-mCherry	Addgene	RRID:Addgene_40270
pIRES-Puro-TCPTP	Addgene	RRID:Addgene_33366
pGEX-2T PTP-1B	Addgene	RRID:Addgene_8602
pBG100-TCPTP	Addgene	RRID:Addgene_33365
Software and algorithms		
GraphPad Prism v9	GraphPad Software, LLC	https://www.graphpad.com/scientific-software/prism/
FlowJo v10	Becton, Dickinson and Company	https://www.flowjo.com/solutions/flowjo
TIMER: Tumor IMmune Estimation Resource	Li et al.[40,90]	https://cistrome.shinyapps.io/timer/
TIDE: Tumor Immune Dysfunction and Exclusion	Jiang et al.[38]	http://tide.dfci.harvard.edu
DAVID 6.8	the Laboratory of Human Retrovirology and Immunoinformatics (LHRI)	https://david.ncifcrf.ov/home.jsp
Living Image 4.7	PerkinElmer	https://www.perkinelmer.com/lab-products-and-services/resources/in-vivo-imaging-software-downloads.html#LivingImage

REAGENT or RESOURCE	SOURCE	IDENTIFIER
Proteome Discoverer 1.4	Thermo Scientific	https://www.googleadservices.com/pagead/aclk?sa=L&ai=DChcSEwjA0t6LjKz9AhW-E9QBHRPQCA4YABAAGgJvYQ&ae=2&ohost=www.google.com&cid=CAESbOD2USsnKiMjDAzZwM6LxIGfBWi64ffTZiJBZN2YYdxx_TEqFouo5IPJi9zr0wn9xejePlAzibf0u4w6Tlw9Ws1Crdz-sG90vej46uoMIBWf32jdSRWfsDFYDjGS_uaGqmrpjd0ra5BgbKzdCA&sig=AOD64_2wys4IciS2LP3we67wA6mtXRAVcw&q&adurl&ved=2ahUKEwj2qNaLjKz9AhUXmmoFHaWfCBgQ0Qx6BAgEEAE&nis=2&dct=1
BioPharma Finder v2.0.1.0	Thermo Scientific	https://www.thermofisher.com/us/en/home/industrial/mass-spectrometry/liquid-chromatography-mass-spectrometry-lc-ms/lc-ms-software/multi-omics-data-analysis/biopharma-finder-software.html